Monash High Powered Rocketry

Critical Design Review

Solaris MkIII

1. Positionality Statement

Monash High Powered Rocketry is an Australian team founded in 2018 by Meaghan Munro. The team has since grown to over 140 individuals. The propulsion team is currently at 20 members and we are working towards IREC25, launching our hybrid engine, Solaris MkII to an altitude of 10,000 ft.

The team has competed in many competitions in the past, launching to altitudes ranging from 5000 ft to 30,000 ft, both within Australia and internationally. The team has performed extremely well and won multiple awards. In 2025, the team will be showcasing our first ever entrant into a hybrid engine category, with Solaris MkII expected to take our rocket Project Zenith to 10,000 ft, and utilise control systems onboard to accurately target an apogee. The motor has 10+ static fires under its belt and Zenith has launched twice, positioning the team strongly for 2025. Solaris MkII is the most powerful and highest impulse SRAD motor in Australia and Monash HPR holds the title of first and largest SRAD hybrid ever flown in Australia (two different engines).

To date, the team has successfully built 4 hybrid rocket motors; Solaris MkI, Bambino, Solaris MkII and BigBino, with Bambino and BigBino being onboarding projects for our two most recent recruitment intakes.

We are currently looking to expand our ambitions to high altitude launch attempts with Solaris MkIII. Solaris MkIII is aiming to be a 10 kN LOX hybrid, this ambitious goal would be helped greatly through the Race2Space competition.

2. Outreach Statement

Monash HPR offers a range of STEM outreach programs and rocketry workshops for primary (Prep – Grade 6) and secondary (Grade 7 – Grade 12) schools across multiple states in Australia. Our workshops are conducted at schools, community hubs, our workspace, and can also be delivered online to suit the needs of the school and allow flexibility for remote sessions. These workshops are designed to showcase the fun and rewarding aspects of STEM (Science, Technology, Engineering, Maths) through hands-on projects that foster interactive learning and engagement. Each session includes an introduction to our team and our work, an overview of rocketry fundamentals, and a hands-on activity. We also tailor presentations for specific events, such as Science Week or other themes connected to Monash HPR.

Our interactive activities range from bottle rocket launches and paper rocket projects to low-power rocket (LPR) demonstrations and OpenRocket workshops for older students. The paper rocket launch is especially popular, as it allows students of all ages to experiment directly with what they've learned in a fun, hands-on way.

As part of Monash Makerspace, an innovative environment at Monash University, Monash HPR regularly collaborates with other university teams, clubs, and faculties to offer tours, presentations, and workshops that explore broader engineering topics, with a focus on aerospace.

In the past year, Monash HPR has performed 38 outreaches, delivering workshops to 15 schools and participating in more than 20 collaborations within the university, reaching over 2,000 students and significantly contributing to STEM education.

3. Mission Statement

Race2Space provides an immense opportunity for the team to take a big step forward and leverage the years of experience we have with a low budget to do something more ambitious.

Monash HPR has worked extraordinarily hard over the last 18 months to develop our current engine Solaris MkII and push the boundaries of what can be achieved by student engineers in Australia. We hope to use this opportunity to further develop our skills by tackling our biggest project yet.

The opportunity Race2Space provides is one that a team like ours never sees and gives us a chance to represent our country and set us up to build an engine capable of taking the team to over 100,000 ft. The team is hoping to break the amateur rocketry altitude record in Australia, and to do that, we will require the support of competitions such as Race2Space.

Using liquid oxygen (LOX) and a high flow rate feed system allows us to test our combustion chamber without the restrictive initial cost of ground support equipment (GSE) and feed systems needed for LOX and/or blowdown pressurisation systems while characterising our combustion chamber and gaining valuable data and knowledge. This engine, Solaris MkIII, prioritises efficiency and mass saving, as this is essential for high altitude launches.

4. Engine Details

4.1 Engine Overview

4.1.1 Previous experience

Solaris MkIII is the team's latest iteration in the Solaris hybrid engine family. This engine as mentioned aims to take the team to 100,000 ft. To do this, the engine is initially designed to produce approximately 10 kN average thrust for 8-10 seconds.

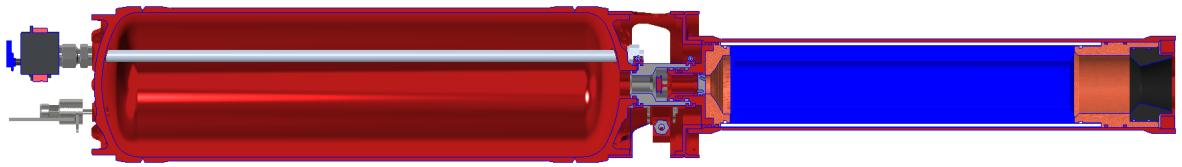

Figure 1: Renders of Solaris MkII, the team's IREC25 entry engine.

This engine builds on Solaris MkII (figure 1), now statically fired 10+ times and flown thrice, the team has a proven track record with complex hybrid engines. The threaded closures used on Solaris MkII will translate to Solaris MkIII (figure 2) along with the familiar pre-combustion chamber and post-combustion chamber design. The biggest changes will be the addition of a composite overwrapped combustion chamber, a water cooled nozzle, resonator, mixing plates, new fuel grain geometry, baffles, fuel inserts, swirl and pintle injectors and a segmented fuel grain. These changes represent a quantum leap in our capabilities and reflect the team's goals to continuously improve and push our own limits.

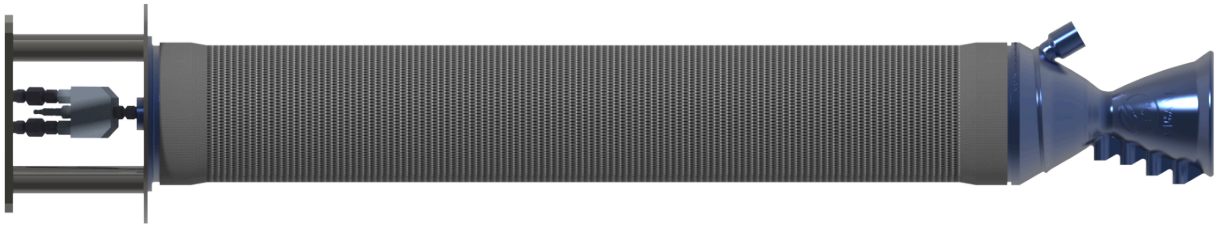

Figure 2: Render of Solaris MkIII combustion chamber

F4.1.1 System architecture

To meet these targets, the Solaris MkIII engine features a water cooled nozzle to handle the long burn time, and it will use LOX as the oxidiser to increase efficiency to support a high altitude vehicle. Further, a composite overwrapped combustion chamber aims to minimise mass and the engine will feature mixing plates to improve combustion efficiency and resonators to minimise combustion instabilities and allow us to push the chamber pressure higher. The design currently features a pressure swirl injector assembly designed to induce maximum atomisation and swirl in the flow. The fuel grain contains a wagon wheel swirl cross-section and consists primarily of paraffin wax with an ABS matrix; these design choices are made to ensure a consistent and high efficiency burn. The post combustion chamber

allows for post-burning of the fuel for further increase in combustion efficiency and the TOP (Thrust Optimised Parabolic) nozzle allows us to take full advantage of our flow. Being a new engine, ports for a pressure transducer in the forward closure will be used as well as ports for thermocouples axially along the nozzle for data and characterisation purposes.

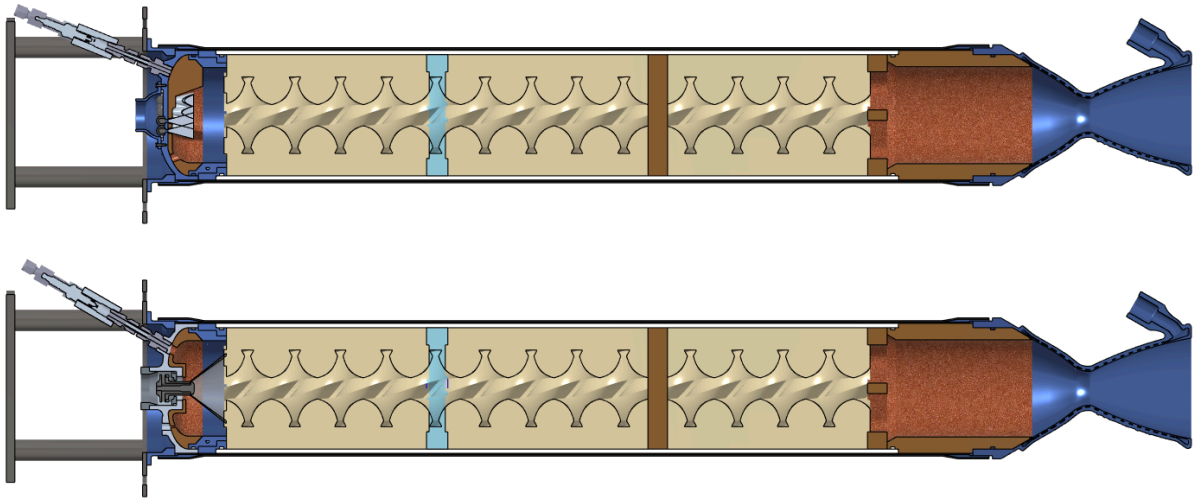

Figure 3: Solaris MkIII cross-section with swirl injectors (top) and pintle injector (bottom)

The structural interface is designed around the AEL J1 test facility and will use the test facility's LOX supply and torch ignitor. The 10 kN thrust requirement means a high thrust load cell and interface will be needed, and the engine will be designed according to the given specifications.

Figure 4: Render of Solaris MkIII combustion chamber

4.2 Structural Interface

4.2.1 Structural Interface Overview

The structural interface is essential and proper care must be taken into its design as it is a critical safety system. The structural interface is a 2 part design consisting of a steel plate with slots to account for engine alignment bolted to the engine adapter made from aluminium 6061 T6, which is threaded to the forward end of the combustion chamber. This assembly will then be secured by bolts to the standoffs provided by the AEL J1 Test Facility. The slots on the steel disk allow for orientation and thus clearance for the fluid lines, ignitor and sensors.

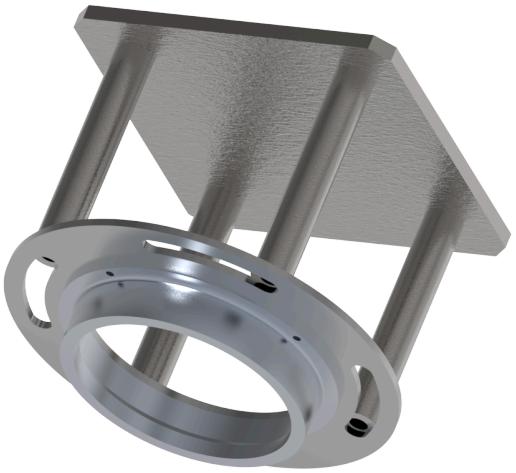

Figure 5: Structural interface render

Further investigation into the strength calculations of the system can be found in section 6.4. The steel plate will be water jet cut on campus while the aluminium threaded section will be machined. Splitting into two parts allows us to keep the stock size reasonable.

In addition, the combustion chamber is supported from the rear end by a floating clamp (figure 6). As all the thrust loading during firing is directed axially into the structural interface, the presence of the clamp serves to resist moment loading from the weight of the engine in addition to maintaining motor alignment.

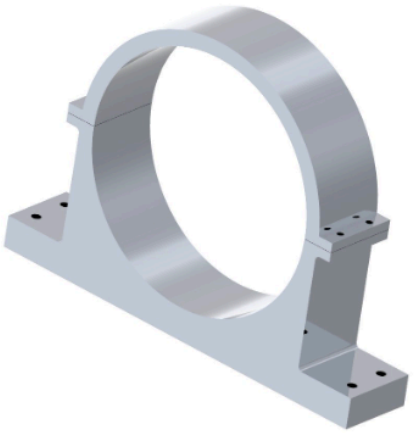

Figure 6: Rear clamp render

4.3 Injector

4.3.1 Injector Overview

The injector is essential in atomising and mixing the oxidiser. The oxidiser of choice is liquid oxygen which is very sensitive to good atomisation and mixing, unlike nitrous oxide, which is very forgiving due to its two phase nature and the energy it receives from thermal decomposition. The team has decided to test two different injector designs: single swirl injectors and a pintle injector. The designs were selected to promote atomisation through liquid film breakup and mixing with the fuel through swirl, therefore offering increased suitability for use with LOX. Two designs are chosen as there is little available research into LOX injector designs for hybrids, so the team is looking to research and compare performance of different designs.

4.3.2 Swirl Injector Configuration

The swirl injector configuration involves a series of stainless steel swirl chambers (black figure 7) that are pressed into the forward closure for the combustion chamber via heating of the forward closure and freezing of the injectors to get an interference fit and seal. Drilled axial holes in the forward closure form the converging nozzles for these swirl chamber inserts. Each swirl chamber has a series of tangential inlets, which are supplied with LOX by a manifold just above the forward closure. The manifold is formed by a manifold plate, and sealed by a spring energized PTFE face seal.

316 stainless steel was chosen as a material for the injectors as it:

- Is compatible with high pressure LOX
- Is high strength
- Is easily accessible

- Has a favourable coefficient of thermal expansion (CTE) to install into and retain the forward closure with a press fit

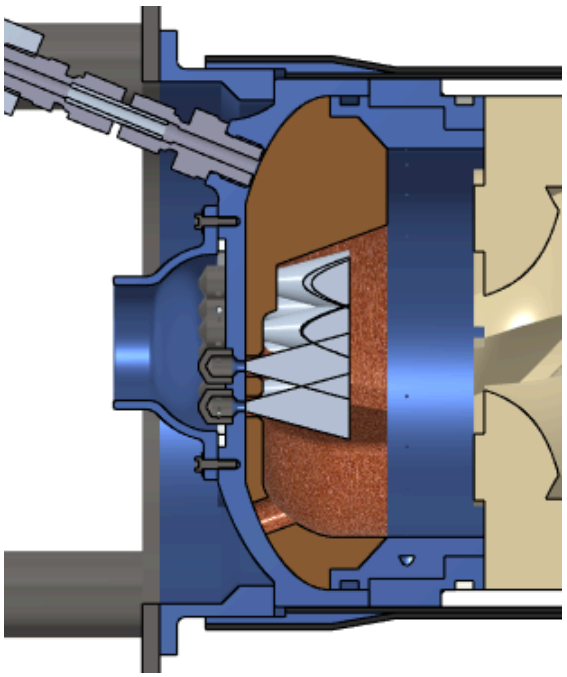

Figure 7: Swirl injector assembly in Solaris MkIII

For assembly of the injectors into the forward closure, the stainless steel injectors will be pressed into the aluminium housing. The difference in CTE between the injectors and the forward closure causes the fit to become tighter with lowering temperature, meaning that at operating (cryogenic) temperatures, the fit will become tighter than at room temperature, allowing for easier installation. A shrink fit will still be performed at room temperature so the injectors are sealed during the initial cool down during a static fire.

Input parameters to the swirl injector design were the required oxidiser type and mass flow, pressure differential, fuel grain geometry and forward closure area. Critical output parameters were film thickness (important for atomisation), spray angle (important for atomisation and fuel grain geometric suitability) and number of injectors. Calculations were performed with a mixture of analytical and empirical formulas. Analytical calculations were used to predict mass flow and spray angle, while droplet diameter was predicted with empirical equations.

The spray angle of the injectors must be suitable for the fuel grain/combustion chamber size in that it must form spray cones that do not contact the fuel grain close to the pre-combustion chamber walls. If the oxidiser flow directly contacts the chamber walls, it has the potential to burn through and cause critical failure of the engine. Given that theoretical models predict spray angle to only be dependent on injector geometry, and independent of pressure differential and fluid density, testing was carried out with 3D printed swirl injectors with a garden hose (see image below) to confirm the accuracy of spray cone angle predictions. It was determined that spray angles were underpredicted by approximately 10 degrees, which

was taken into account in modelling spray cones in CAD. Geometry was tuned to confine the predicted spray cones to within the fuel grain “wagon wheel” arms.

Figure 8: One test of a 3D printed swirl injector.
Predicted angle: 39.2°
Measured angle (from image): 43.0°
Error: 9.7%

It was found that due to empirical models’ dependence on film thickness for atomisation, increasing the number of injectors lowered the predicted empirical mean droplet diameter of the swirl injectors. Due to manufacturing limitations and packing efficiency, it was determined that 12 swirl injectors was optimal. Adjusting inlet geometry and swirl chamber diameter to meet the mass flow and spray angle requirements, empirical models give between 10-25 μm for droplet diameter. A maximum distance for liquid film breakup of 30 mm was also visually established from this testing. This was established as a maximum due to the tested fluid of water having a significantly higher surface tension than LOX. This 30mm breakup length is what is represented by the spray cones seen in CAD models, and was deemed sufficient for atomising the oxidiser before the separate spray cones from other injectors impinge.

A pattern of injectors was chosen to allow three-spoked baffles to divide the injectors into three sections, as seen in figure 9 below.

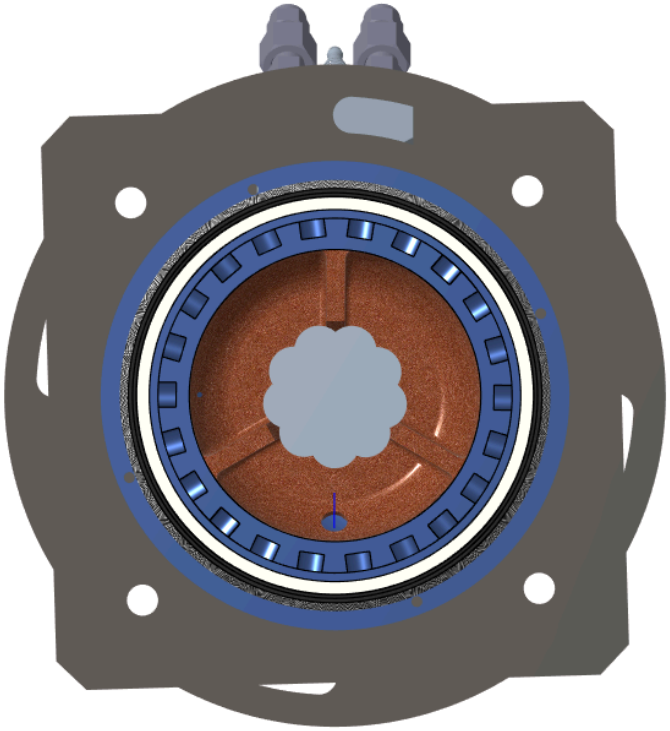

Figure 9: Bottom-up view of swirl spray cones inside baffles

4.3.3 Pintle Injector Configuration

Pintle injectors are known for their inherent combustion stability and good atomisation in liquid engines. An internal radial flow impinges on an external axial flow, creating sheets of liquid film and droplets. A radial gap-type pintle injector was chosen over a radial orifice-type for its even oxidiser distribution around the pintle tip and machinability. Figure 10 shows the pintle injector inside the forward closure with the nested chambers to create the perpendicular flows. The shoulders of the forward closure and the injector act as a split housing for a spring-energised PTFE seal, rated for LOX applications.

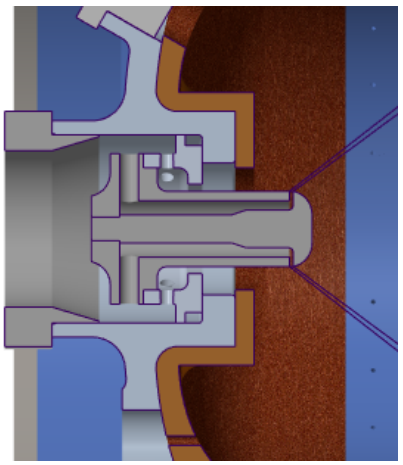

Figure 10: Render of the pintle injector assembly

The major design considerations for this injector are the radial gap and annular gap widths. Each gap was calculated using a sizing script with inputs from the thermodynamic simulations. Gap dimensions impact the resulting spray cone angle which must be scaled to prevent oxidiser interference with the resonators. The spray cone is calculated to contact the fuel grain inside the maximum fuel grain port diameter, as shown in figure 11.

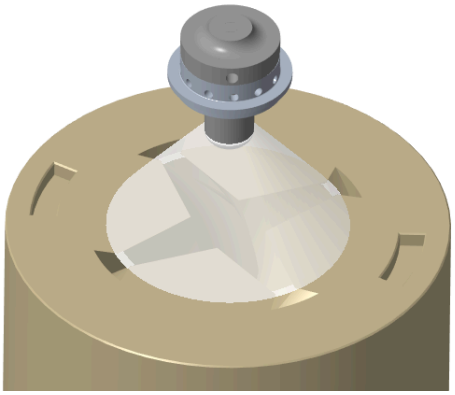

Figure 11: Render of the pintle spray cone contacting the fuel grain

Most of the injector components will be manufactured from 316 stainless steel, specifically the central pintle post that will be in contact with the hot combustion gases. The outer chamber and forward closure will be made from aluminium 2011 T6, which has good LOX compatibility, furthermore it will be anodised for better corrosion resistance. These parts will be insulated by the phenolic pre-combustion chamber and so do not need to withstand the heat of combustion.

4.4 Forward closure

4.4.1 Forward Closure Overview

Solaris MkIII features sensors on the forward closure and the nozzle in conjunction with the thrust data from the test facility. Each forward closure contains a pressure transducer port for chamber pressure through a ¼” BSPT port. Furthermore, there is a blind ¼” BSPT hole for measuring the temperature at the centre of the forward closure to better characterise the temperature distribution as a result of the LOX passing through the forward closure and the heating from combustion.

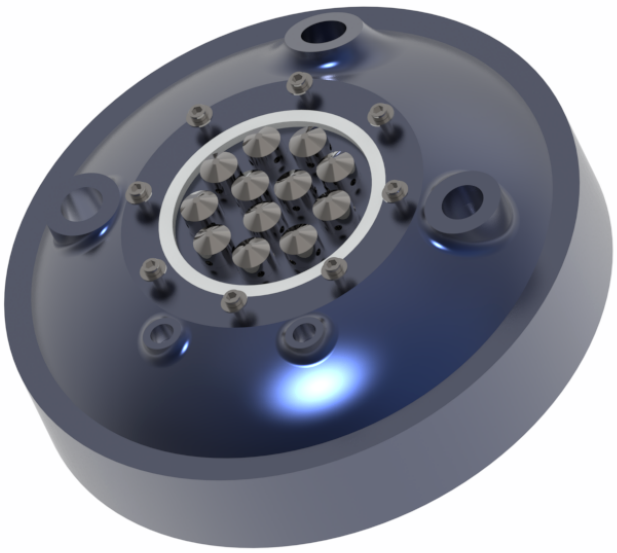

Figure 12: Render of swirl injector assembly in forward closure

Both forward closures also feature an angled port to direct ignitor gas into the injector stream. The AEL torch ignitor as well as our own torch ignitor use the same G ¼ BSPP fitting. There are two adjacent 6 mm dowel holes with matching blind holes in the pre-combustion chamber/baffles, these serve as locating features when assembling the engine, once the engine is assembled they are removed and plugged with taper thread grub screws.

For the material selection of the forward closure, an aluminium alloy was desirable due to the material's relatively high strength and low density, ideal for it having many non-structural surfaces. Aluminium alloys are also easily available. However, careful consideration was taken in choosing the exact type of alloy to use, as many aluminium alloys contain elements that are reactive with liquid oxygen, and in the event of mechanical ignition promotion (e.g. sudden pressure change from startup flow) can be ignited. Of the particular alloys tested by NASA for ignition with LOX, appropriate alloys are not available in Australia. However, the 2024 alloy tested and passed by NASA to appropriate pressures is similar in composition to the commonly available 2011 alloy. Therefore the aluminium 2011 alloy was settled on for use with the forward closure and other aluminium components in direct contact with supply pressure LOX. Furthermore these components will be anodised, which is a very good compatibility with liquid oxygen.

4.5 Nozzle

4.5.1 Nozzle Overview

Due to the extended burntime, this engine is designed to address concerns about the condition of the nozzle under such thermal loads. As a result, cooling of the nozzle has been explored on this engine. The nozzle will feature a converging and diverging section with a throat of 39 mm to ensure the combustion gases are choked at this region. The exit to throat area ratio is 9.6 as determined by calculations run by the team's custom hybrid rocket engine simulation software and verified by Rocket Propulsion Analysis (RPA). The nozzle material is AlSi10Mg, in future the nozzle will be made from GRCop-42, a copper alloy, however, our supplier does not currently have this material in stock. In the current configuration, the nozzle will be water cooled utilising helical cooling channels as well as film cooling.

Figure 13: Render of cooled nozzle

The nozzle contains 4 thermocouples ports for type K thermocouples to be mounted using a 5 mm to ⅛" BSPT compression fitting with the 5 mm sheath on the thermocouples. The values obtained from these thermocouples will be used to validate our simulations and won't be featured on the flight configuration.

4.5.2 Thermal simulations

Some thermal simulations were conducted using RPA and Ansys Fluent.

4.5.2.1 Water

The nozzle will be cooled with 1.3 kg/s of water at 75 bar using the IPA pump, as per AEL specifications. Using AlSi10Mg means the nozzle must be kept at low temperatures to maintain a sufficient yield strength, channel cooling alone is not enough to achieve this so film cooling in the nozzle top manifold and near the throat will be used. 0.45 kg/s of water will be used for film cooling in the manifold and 0.27 kg/s in the throat, keeping the nozzle at a maximum temperature of 440 K. This equates to 16% film cooling compared to the total engine mass flow rate. Using a large mass flow rate through a single set of film cooling holes ensures the holes can be made large enough (0.55 mm minimum) to print and service. The hot side will be 1.3 mm thick.

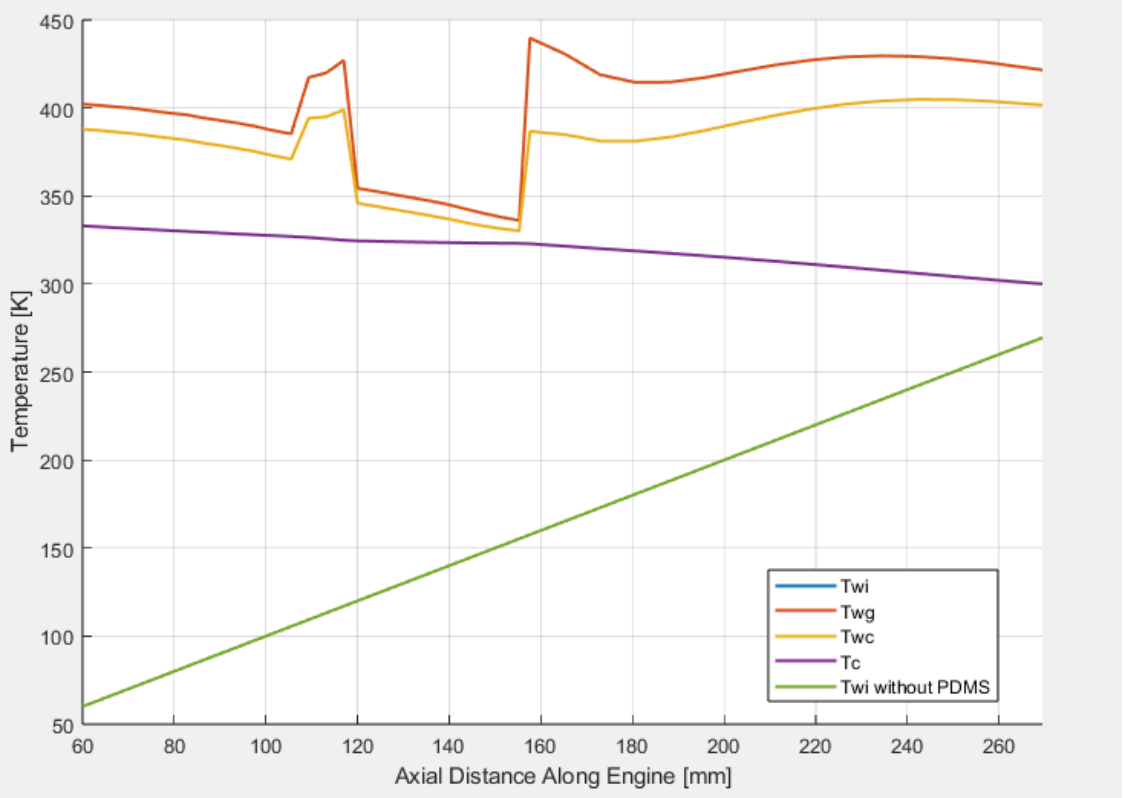

Figure 14: Temperature at different points in the nozzle vs axial distance along the nozzle for water cooled nozzle

A minimum factor of safety of 2 is simulated on the nozzle (figure 14), which is within the team's internal requirements of 2 for a metallic component. To determine the stresses on the nozzle, MATLAB code from Bristol SEDS is used. The results from RPA and the stress calculations can be found in more detail in 6.6.2.

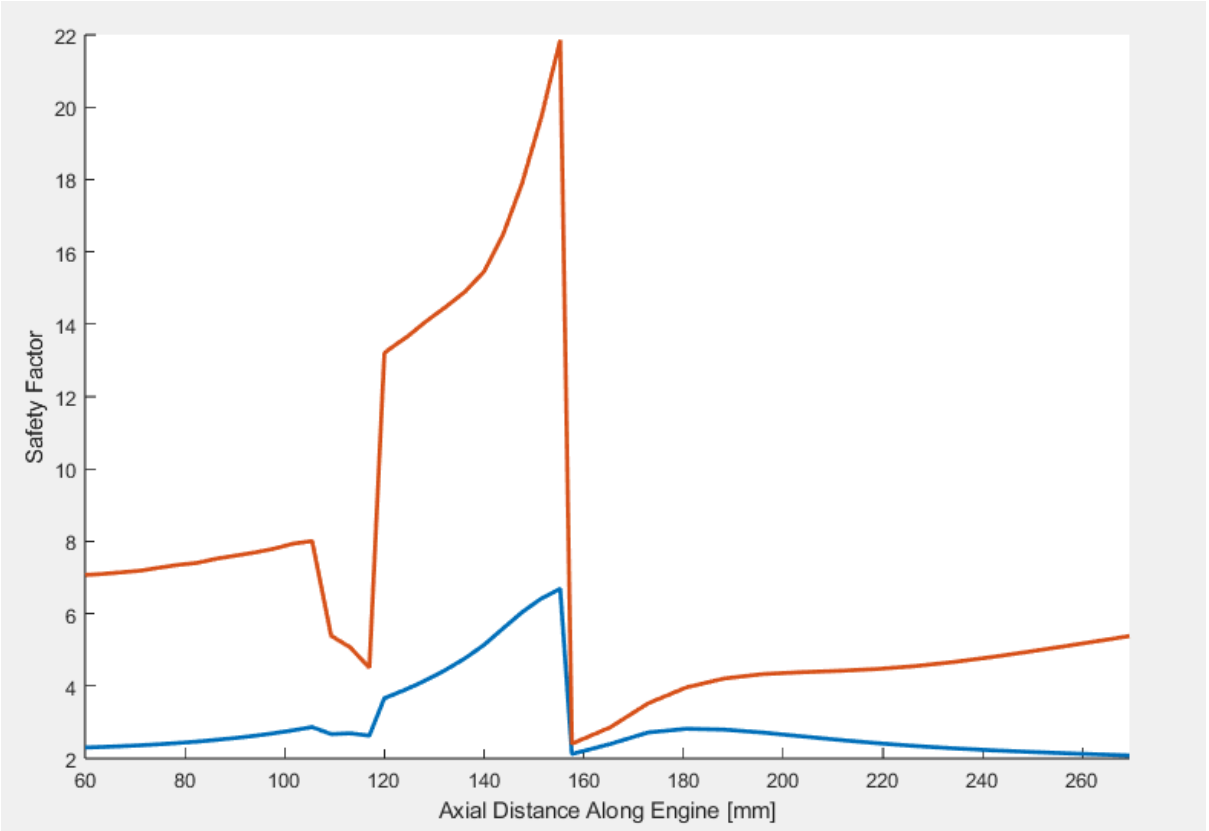

Figure 15: Factor of safety of nozzle vs axial distance along the nozzle for water cooled nozzle

Calculations have been done with the 8 kg/s at 20 bar provided by AEL, however this specific configuration cannot sufficiently cool the nozzle with just channels, film cooling can be used to achieve the temperatures desired. The issue with the low pressure configuration is the water pressure is lower than the chamber pressure and it is unsure whether this will result in the combustion gases getting into the nozzles or the water being pulled out of the nozzle due to entrainment, which is what would be desired.

Using the IPA feed system with the water at high pressure allows the nozzle to be film cooled safely, thus this is the option that is being used going forward.

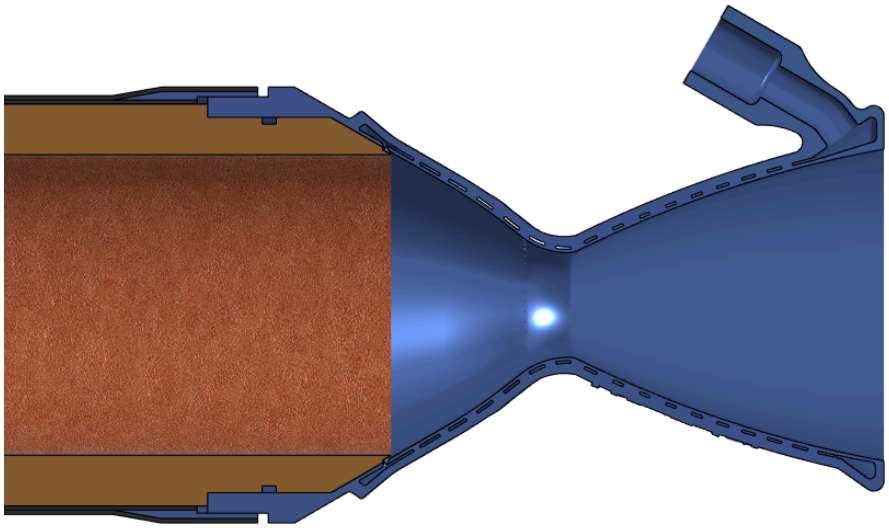

Figure 16: Interface of nozzle and post-combustion chamber

Initial CFD has been done on an older iteration of the nozzle with water (see 6.6.1 for detail). Going forward, the latest version will be simulated and compared against RPA for consistency. Using water at 20 bar with regenerative only, the maximum temperature of the nozzle was found to be 620 K, providing some consistency with the RPA simulations for this nozzle. This workflow will provide insight into pressure losses and velocities in the channels and will help us optimise our manifolds.

4.5.3 Manufacturing

Monash Centre for Additive Manufacturing (MCAM) will be printing this nozzle. The confirmed date for printing is the 28th of April, with scope for a second nozzle to be printed as well. The de-powdering process will involve using their shaker pad that rotates the components and vibrates it to dislodge powder. Furthermore, they will heat the nozzle and pass cold air through it and thermal image it, any blockages in the channels should be identifiable from this, this will also be a method to further de-powder with just the gas pressure. X-ray or CT scanning is something that would be beneficial as well and the team has been investigating the use of an on campus machine to assist with this.

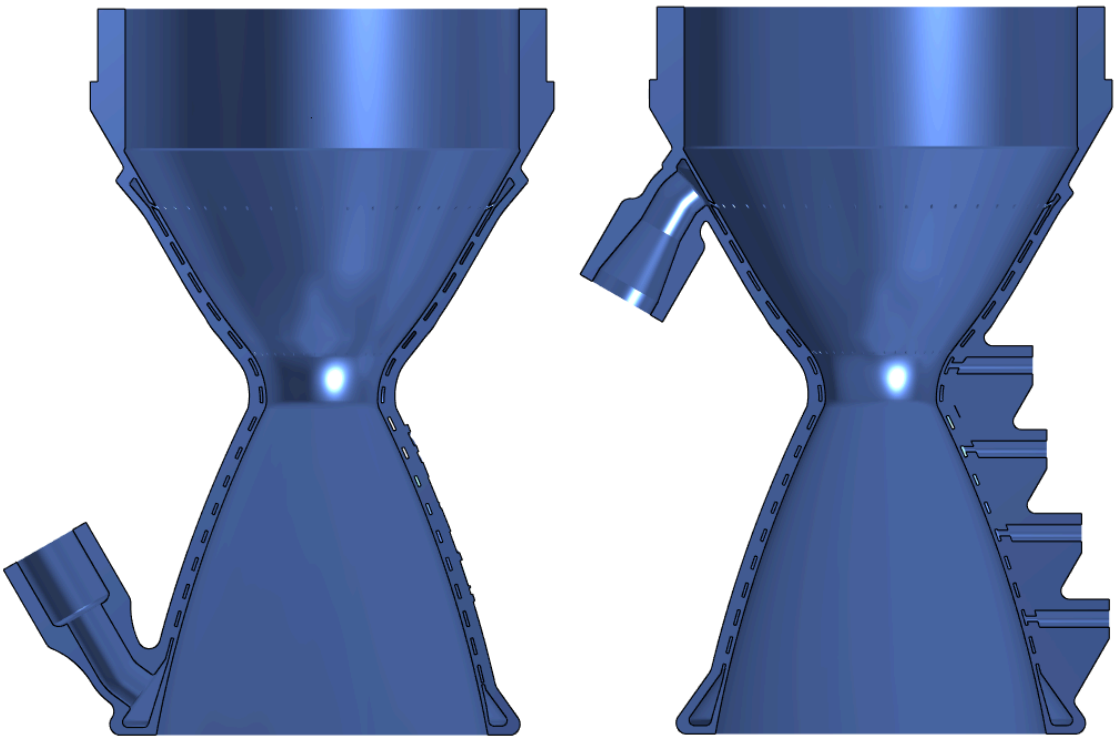

Figure 17: Cross-sections of nozzle at 90 degree offsets

The thermocouple ports will be printed at 6 mm diameter and then drilled to 8.3mm to tap ⅛” BSPT (figure 17, right). The 6mm print size is the largest horizontal hole the manufacturers can print. The top manifold port features a print support for printability as well not present in the above figure. Lastly, a support structure creating a pad around the top manifold will be used to decrease the chance of recoat defects around that overhang. The inlet and return lines both feature ¾” BSPP ports.

4.6 Combustion Chamber Wall

4.6.1 Combustion Chamber Wall Overview

Solaris MkIII features a composite-overwrapped pressure vessel (COPV) for the combustion chamber. The chosen design is a Type V COPV, that is, a pressure vessel made up entirely of composite materials, except for the threaded couplers made of aluminium. The pressure vessel consists of several key components. The inner layer is made of fibreglass - to act as a thermal barrier and ablative against combustion gasses in case of leakage. The pressure loading is supported by carbon fibre twill layers forming the bulk of the pressure vessel, the outer layer of the COPV is then covered by a protective carbon fibre sleeve layer to provide abrasion resistance. The fore and aft ends of the chamber pressure vessel will attach to the forward closure and nozzle respectively by means of AL7075 T6 threaded couplers chosen for strength. Since the couplers do not come in contact with LOX, there is no concern with compatibility, which 7000 series aluminium has issues with.

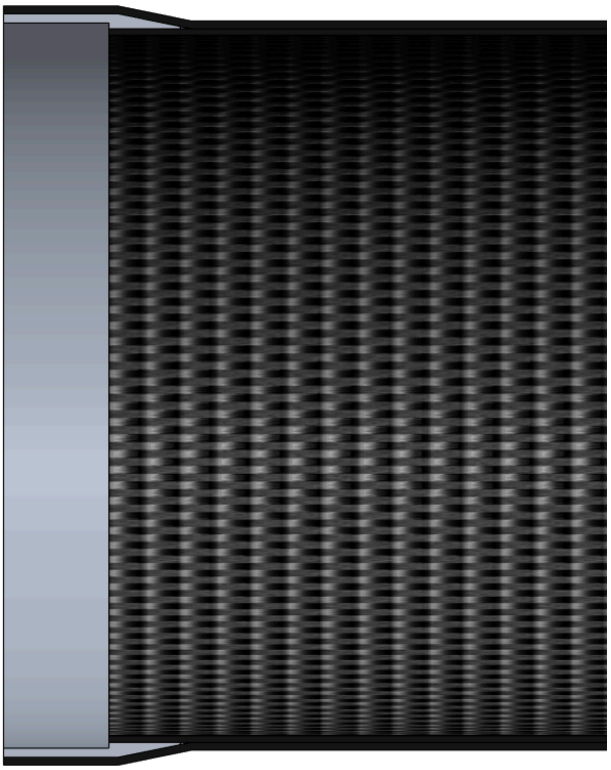

Figure 18: Cross-section of COPV

As this engine will be used on a future launch vehicle, mass reduction is a key design consideration. For this reason a composite overwrapped design was selected for the combustion chamber, as opposed to a more traditional monolithic metallic design. By opting for a Type V COPV, the mass saving is maximised (66% mass reduction compared to an aluminium-walled chamber), as no bonded metallic or polymer liner is needed to provide chemical resistance to the inner layer of the chamber pressure vessel. Instead, the fuel grain's PVC liner serves the dual role of insulating the chamber walls and protecting them against chemical degradation from exposure to the highly oxidising combustion environment.

4.6.2 Manufacturing Considerations

Figure 19: Render of combustion chamber wall with threaded couplers

Various manufacturing techniques were considered, including filament winding using carbon fibre tow material, automated fibre placement (AFP) and various manual techniques (resin-infusion, prepreg layup, wet layup). Ultimately, a wet-layup technique was selected as Monash HPR has experience manufacturing airframes with this method. Further, we were limited by difficulty sourcing high-temperature resistant resin-impregnated carbon fibre fabric or tow. Although we were not able to gain access to filament winding or AFP equipment in our short timelines, our team aims to explore these options in further iterations of this design, in order to gain experience using these industry-standard composite manufacturing methods.

To begin the layup process, a mandrel will be prepared with adequate non-stick coatings prior to beginning the layup. The epoxy system selected for this application is the Technirez R2600 resin with H2409 hardener. This combination was selected as it provides adequate working time and viscosity, while also yielding a very high glass transition temperature of up to 180°C post-cure. Having such a high glass transition temperature provides some margin for temperature increase in the chamber walls due to conduction throughout the burn. A bottom layer of fibreglass twill will also be included in the ply stackup to provide added thermal insulation (in addition to the PVC thermal liner). Paper was also considered as an economical insulating layer, however concerns arose surrounding charring/burning of the paper during the elevated temperature curing cycle.

Above the fibreglass, five layers of carbon fibre twill will be applied. To prevent the buildup of air bubbles during manufacturing, the stackup will be subject to a vacuum for debulking prior to attaching the couplers. The couplers will be made of the Al7075 T6 alloy for its high strength, allowing the M158x2.0 ↧16 threads attaching the chamber to the forward closure and nozzle to have a factor of safety greater than 2. The couplers will be machined in-house using manual and CNC lathes, the 3 pin method and go-no-go threads will be used to ensure the couplers are within specification. The surfaces of the couplers will be roughened via hand-sanding to improve adhesion to the epoxy resin. After attaching the couplers to the

partially-completed chamber, the next 6 layers of carbon fibre twill will be applied, followed by the carbon fibre sleeve. This sleeve is designed to act as a protective layer for the underlying load-bearing twill.

After completing the stackup, the entire chamber will be wrapped in heat-shrinking FEP film. This material was selected for its non-stick properties. The entire assembly will then be prepared and subject to vacuum for the 24 hour cure period at ambient temperature. Subsequently, the chamber will be put into the Monash University autoclave for a high-temperature cure profile as shown in figure 20.

THERMAL CHARACTERISTICS (Tg)		
	H2403	H2409
+ 8 hrs @ 50°C*	75°C	75°C
+ 8 hrs @ 50°C + 3 hrs @ 90°C*	112°C	111°C
+ 8 hrs @ 50°C + 3 hrs @ 90°C + 3 hrs @ 120°C*	143°C	132°C
+ 8 hrs @ 50°C + 3 hrs @ 90°C + 3 hrs @ 120°C + 2 hrs @ 150°C*	157°C	155°C
+ 8 hrs @ 50°C + 3 hrs @ 90°C + 3 hrs @ 120°C + 2 hrs @ 150°C* + 1hr @ 200°C*	160°C	177°C
+ 8 hrs @ 50°C + 3 hrs @ 120°C + 2 hrs @ 150°C + 1hr @ 200°C* + 1hr @ 220°C*	160°C	180°C

** Post cure schedule Tg: by DSC*

Figure 20: Curing temperature data for Technirez R2600 epoxy system

Initial concerns about the aluminium couplers losing strength during the high-temperature curing cycle were taken into consideration. As the high temperature portions of the cure are only for short periods of time, the AL7075 T6 alloy's strength reduction is negligible (see figure 21). Furthermore, thermal expansion/contraction during the curing process is within acceptable limits.

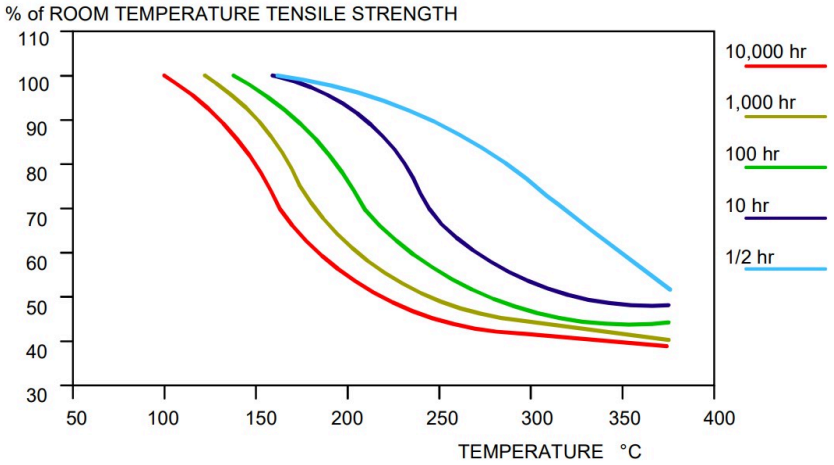

Figure 21: Strength reduction of aluminium alloy at temperature over time

4.6.3 Combustion Chamber Carbon Fibre Wrap

A key consideration is the risk of wrap delamination which may result due to an inadequate layup, leading to air pockets or dry fibres. As the team does not currently have access to a filament winder or automated fibre placement machine, the layup must be done perfectly by hand, ensuring the correct ratio of resin to fibres and ensuring the fibres are not frayed or damaged during the layup, which would decrease overall tank strength. Further physical analysis of the layup methods and techniques is required to understand best practices as well as material properties followed by physical validation testing, this will be supported with extensive use of Finite Element Analysis using Ansys Composite PrepPost software to simulate the chamber and better understand its theoretical structural properties.

Physical testing will also be conducted to investigate the performance of composite overwrapped pressure vessels at varying operating temperatures. In particular, the use of high-temperature resins will help the COPV to retain strength at the elevated temperatures experienced throughout the burn. As shown in the below figure, carbon fibre reinforced plastics (CFRP) experience severe strength reductions well below carbon's melting point of 3,550 °C. This is due to the matrix material's strength reduction when approaching the glass transition temperature.

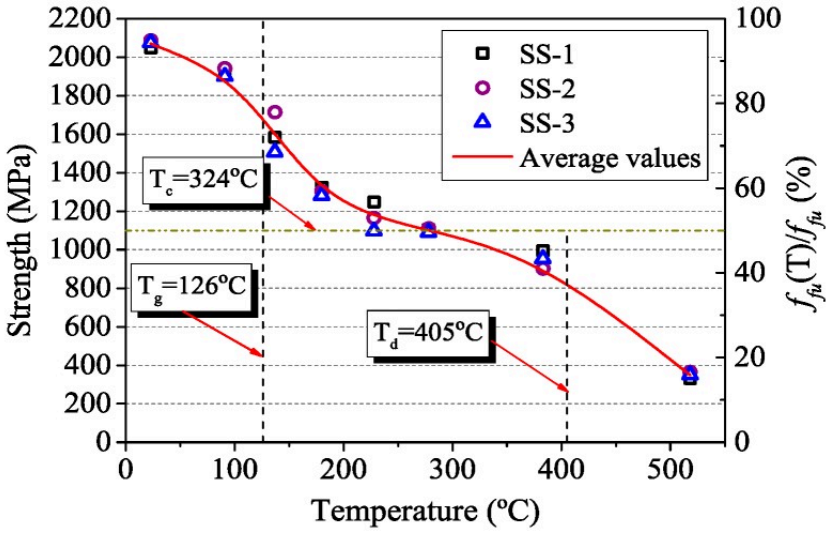

Figure 22: Diagram of CFRP strength vs temperature

Tensile tests will be performed at elevated temperatures to characterise the strength drop-off of our in-house manufactured CFRP materials prior to manufacturing a full scale tank. Subsequently, hydrostatic leak and burst testing will be conducted to verify FEA/ACP simulation results.

4.7 Fuel Grain And Liner

4.7.1 Fuel Grain Overview

The fuel grain is manufactured in 3 segments, each with a wagon wheel swirl fuel grain geometry to ensure constant burn area and constant thrust throughout the burn. The engine will use a paraffin fuel grain within a 3D printed ABS matrix with gyroidal infill, this gives support to the paraffin, allowing us to take advantage of the energy density paraffin wax provides without losing structural integrity.

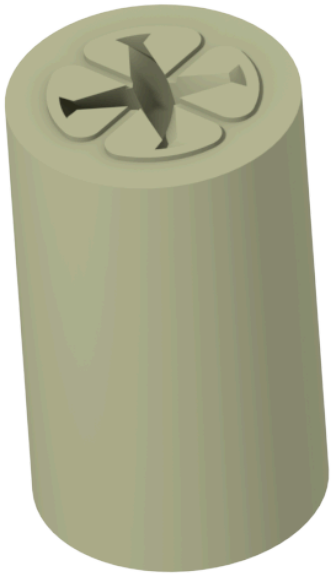

Figure 23: Render of the fuel grain with the wagon wheel cross-section

The fuel grain will be positioned such that the spokes of the wagon wheel line up with the holes in the mixing plate. This is to reduce the amount of oxidiser impacting the top of the fuel grain and to optimise the amount of oxidiser entering the port of the fuel grain. The fuel grain will be positioned with the use of an imprint of the mixing plate spokes on the fuel grain as seen in figure 24.

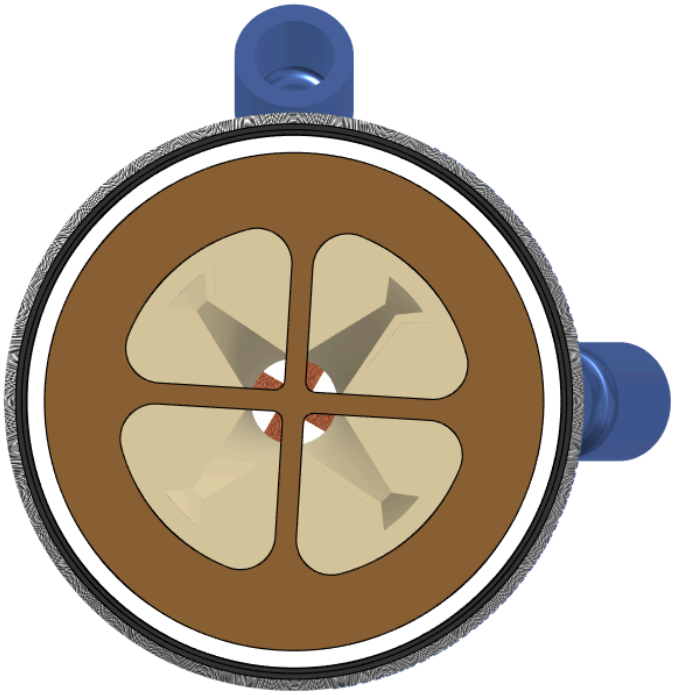

Figure 24: Cross-section view of fuel grain integration with mixing plate

4.7.2 Liner Overview

In order to protect the combustion chamber from heat and combustion gasses a liner will be placed in between the fuel grain and the wall of the combustion chamber. The fuel grain should not burn completely through, however, in the case that it does, the liner will be in place to mitigate the risk of damaging the chamber wall. In the event of the fuel grain burning completely through the PVC will act by regressing far slower than the paraffin and ABS which will allow the oxidiser enough time to be depleted before exposing the chamber walls to combustion gasses. The liner is designed to seal with the resonator and post-combustion chamber using o-rings to seal combustion gasses (figure 25). The liner will be one section and the chamber stack up will all seal on the internal of this. PVC also has strong compatibility with LOX, unlikely to spontaneously combust.

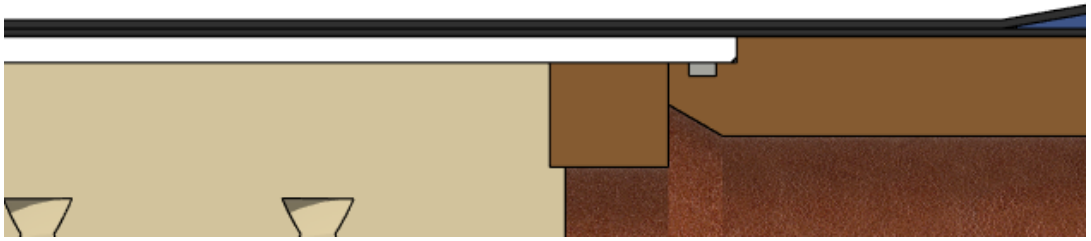

Figure 25: Integration of PVC liner with post-combustion chamber, mixing plate and fuel grain

4.7.3 Manufacturing Considerations

Figure 23 shows the suggested geometry for one of the segments. Segmenting the fuel grain was initially chosen to accommodate the limits of the team's 3D printers. However, this also provides an opportunity to include mixing plates between the grain segments to control mixing throughout the combustion chamber. The team's previous engine, Solaris MkII, showed evidence of axial regression which will be exacerbated with a longer fuel grain (360mm vs 705mm). The mixing plates may allow us to mitigate this issue while increasing the combustion efficiency. Previous paraffin fuel grains have shown cracking and warping due to thermal expansion during the curing process, this will be mitigated by controlling the cooling of the fuel grain to approximately 1 °C/min using a custom heat box. PVC pressure pipe is not sold with the needed outer diameters or length. Pipe will be cut down to size and turned on a lathe to achieve the desired outer diameter.

4.8 Mixing Plate

4.8.1 Mixing Plate Overview

The engine utilises two mixing plates positioned behind each fuel grain section to assist in mixing the fuel and oxidiser. Each mixing plate uses the same four-spoke design shown in Figure 26, which helps to displace the central column of oxidiser that would otherwise not react with the fuel and to introduce turbulence which further increases mixing.

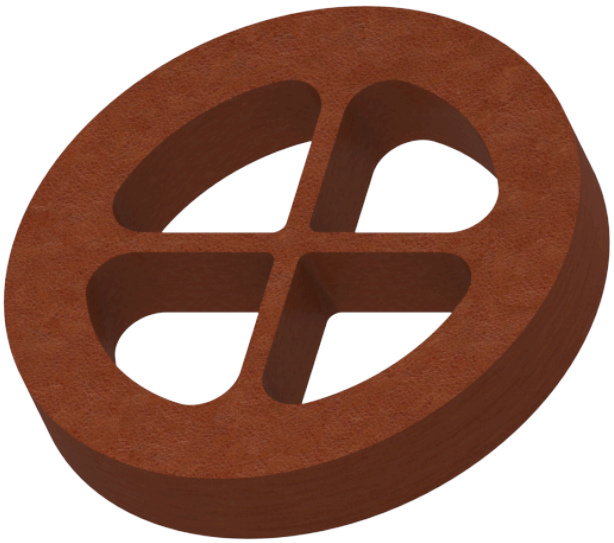

Figure 26: Renders of the mixing plate showing the four-spoke design

The spokes are sized so that they do not restrict the area of the fuel grain's port to below 1.5 times the area of the throat. This provides a safe margin so that in the event of a higher than expected pressure startup, the flow will not be choked before the throat of the nozzle. A

particular orientation with respect to the fuel grain is needed to not drop below this area ratio, hence keys are included which interface with the slots in the fuel grain sections.

The mixing plates do not require any direct sealing. The two plates hence act as dividers between the fuel grain sections, the compression from the nozzle and engine adapter will ensure a good fit between all the components..

Having two of these mixing plates also has the advantage of decreasing the effects of axial regression. A long fuel grain will be prone to regression rates falling off along the axial direction, however the increased mixing caused by each of these parts will increase the regression of the fuel grain immediately downstream of it. Each of the plates is intended to lift the regression rate back up for the fuel grain section in front of it, hence resulting in more uniform regression throughout the whole combustion chamber.

The chosen material for the mixing plate is cloth phenolic due to its ablative properties which allow for the material to withstand combustion conditions for short periods of time. This part is not intended to be reusable, hence ablation is able to be used as a thermal management method to take heat away from the part. In order to reduce the ablation that occurs, a ceramic coat is also applied to the mixing plate, which is intended to increase the time that ablation takes to affect the part by insulating the outer surface.

4.8.2 Mixing Plate Simulation

The strength of the mixing plate was analysed through the use of CFD and FEA. As the maximum force exerted on the plate is expected to be during the initial injection of LOX during startup, CFD was performed on this injection process where the pressures on the top and bottom surfaces of the plates was recorded. This simulation gave a maximum pressure differential of 21 bar as depicted in Figure 27.

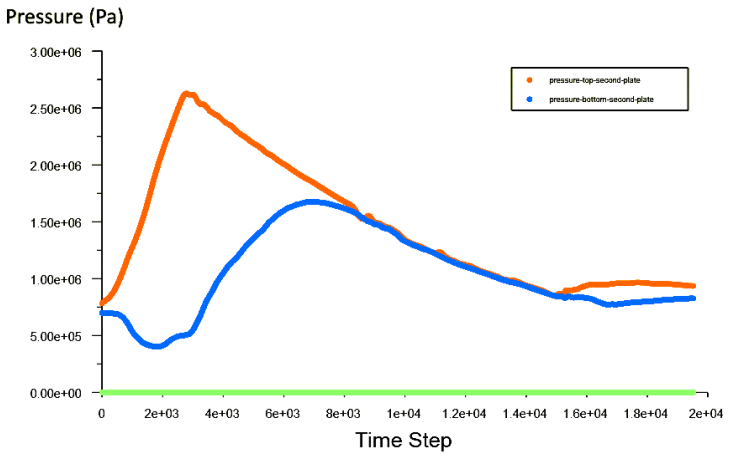

Figure 27: Surface pressures on the top and bottom surfaces of the second mixing plate during initial injection of LOX, with a maximum differential of 21 bar.

During FEA, these pressures were applied to the area of the mixing plate that protrudes into the port. Supporting the plate by the outer 5 mm on the bottom surface, as is the case for the bottom mixing plate, gives a maximum stress at the bottom of the intersection of the spokes, seen in figure 28. This gives the mixing plate a minimum factor of safety of 5.4.

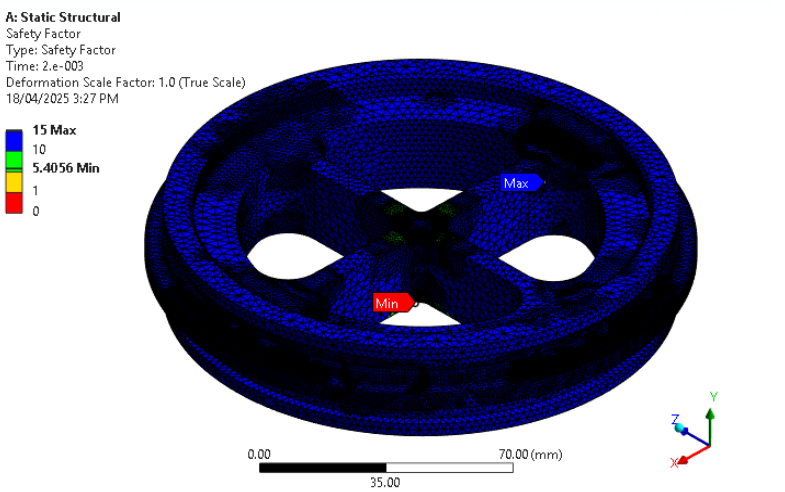

Figure 28: Ansys FEA of the mixing plate with a minimum FoS of 5.4.

This high FoS is used due to the expected loss of material during combustion which will weaken the part, however the forces on the plate later in the burn are not expected to be as extreme as startup. Additionally, this material is only rated to a continuous temperature exposure of 120°C, meaning that the high combustion temperatures are expected to slightly weaken the material during an 8 second burn.

Further simulation was also conducted on the ability of the mixing plate to induce turbulence into the combustion chamber flow. A 3D, multiphase, steady state simulation was performed within Ansys Fluent. Liquid oxygen was injected into a chamber initially filled with air, with results showing regions of recirculation around the mixing plate and other devices such as the fuel insert (section 6.8). A 2D axisymmetric, multiphase, transient analysis was also performed in order to record the pressures on the mixing plate that were used during FEA.

4.9 Pre-Combustion Chamber/Post-chamber

4.9.1 Pre-combustion chamber/Baffles overview

The baffles have been designed to complement the Helmholtz resonator, discussed in Section 4.10, by targeting lower-frequency combustion instability modes that the resonator itself is not sized to mitigate. Their integration helps to broaden the range of instability suppression, especially in hybrid rocket engines where instabilities caused by the first tangential mode are commonly observed. Research supports that baffles with fewer than four

spokes are most effective at reducing this particular mode. Consequently, the design includes a three-spoke baffle, as seen in figure 29 below.

These baffles are specifically intended for use with the swirl injector configuration, as they provide no functional benefit to a single pintle injector. When paired with the swirl injector, the baffles will also serve a dual purpose as a pre-combustion chamber, helping to simplify the design and reduce the overall part count. To withstand the harsh conditions of a full-duration burn, the baffles will be constructed from phenolic, a material known for its high thermal resistance and historic use in pre-combustion chambers. Additionally, the baffle's top surface has been designed to act as an insulator and shield the forward closure from combustion gases. There is an angled port to interface with the AEL J1 test stand's torch ignitor if required.

To ensure the baffles will not disrupt the oxidiser spray cones, the tapered sections of the spokes have been carefully shaped to avoid interfering with the injector's spray cones. The baffles also sit flush with the inner diameter of the Helmholtz resonator. The baffle height reaches a maximum of 25 mm, which aligns with research that baffle height should be at least 20% of the chamber diameter (112 mm in the pre-chamber).

Figure 29: Render of swirl injector pre-combustion chamber

Since the use of a single-port injector renders baffles unnecessary, a second pre-combustion chamber will be manufactured for the pintle injector assembly. It features a similar curved profile to the baffles and is also made from phenolic for its insulating properties. The shoulder of the pre-combustion chamber is not structural and exists to protect the forward closure and the injector from the combustion gases. Drilled holes will be added to allow the sensors access to the chamber environment and to interface with the torch ignitor.

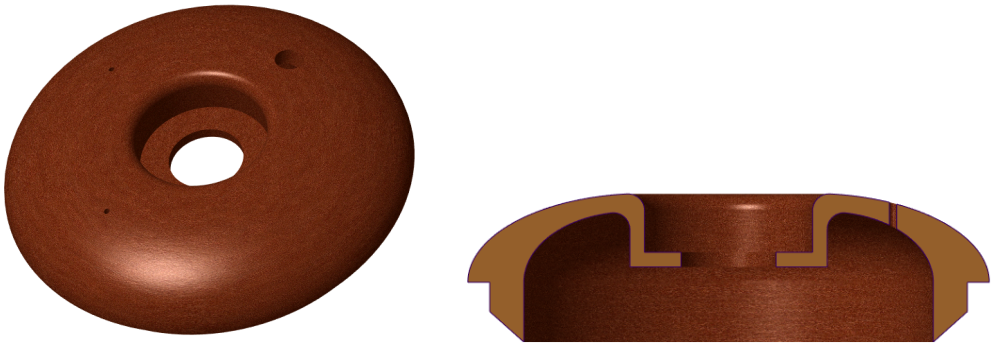

Figure 30: Renders of pintle injector pre-combustion chamber

Like the baffles, it will interface with the Helmholtz resonator, which will seal to the forward closure using the standardised o-rings and backup rings used by the rest of the combustion chamber.

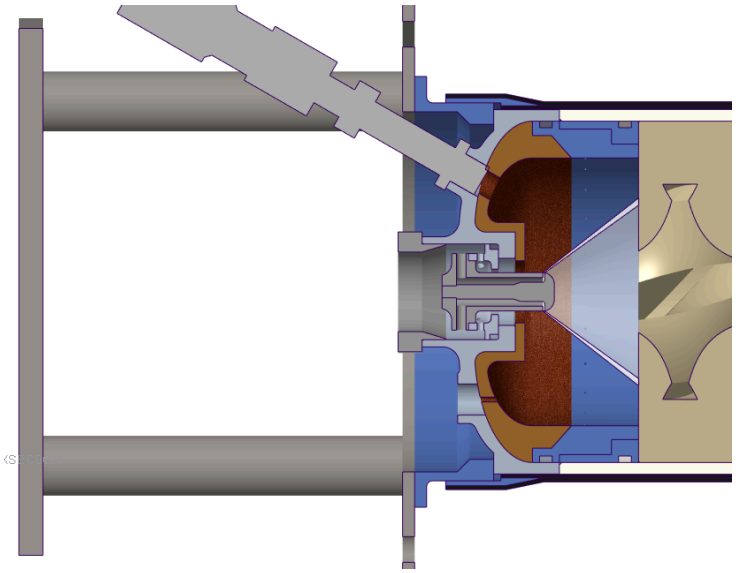

Figure 31: Render of pintle pre-combustion chamber integrated with forward end of chamber.

4.9.2 Post combustion chamber overview

The post combustion chamber serves as a zone aft of the fuel grain that allows for complete combustion of the propellants. Figure 32 shows increasing L/D ratio results in an increase in combustion efficiency. The post-combustion chamber has an L/D of 1.5. Reasoning for this is directly pulled from figure 32.

Table 4 Comparison of the post-chamber effects on the three motors

Parameters	Test (1) (base line)	Test (2) (L/D = 1.0)	Test (3) (L/D = 1.5)
Chamber pressure [bar]	12.2	12.9	13.3
Thrust [N]	8.6	9.9	10.568
Average mixing ratio	3.8	3.7	3.8
Average regression rate [mm/s]	0.108	0.109	0.107
Experimental c* [m/s]	1324	1398	1444
Theoretical c* [m/s]	1525	1529	1525
Combustion efficiency %	87	91	95
Specific impulse [s]	127.9	146.1	156.0
Characteristic length [m]	7.5	20.6	27.1

Figure 32: Comparison of different L/D for post-combustion chambers

Like the pre-chamber, the post-chamber seals with two o-rings. It also features lead in and lead out chamfers for a smoother flow transition. Figure 33 shows a lip at the top of the post-chamber which is used as a way of mating the post-chamber to the mixing plate for sealing and support. Also like the pre-chamber, the post-chamber is made from phenolic for the same reasons.

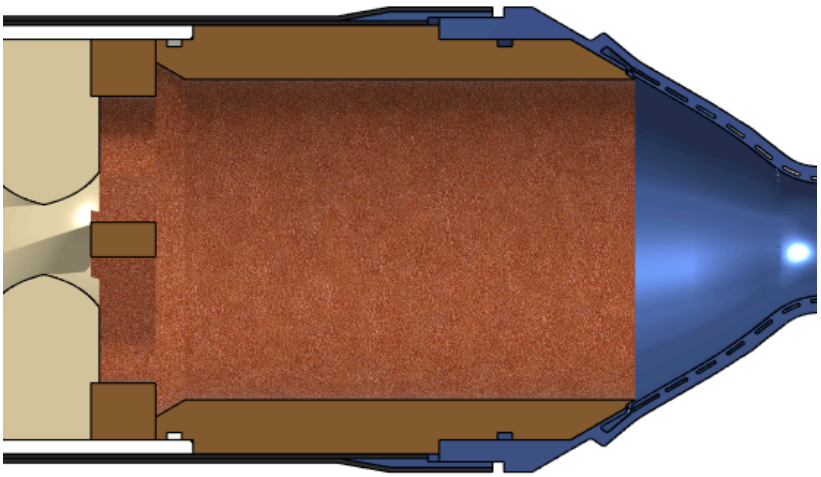

Figure 33: Renders of post combustion chamber integrated with aft end of chamber

The threaded nozzle post-combustion chamber configuration (figure 33) allows for the post-combustion chamber to be extended to meet the nozzle. The post-combustion chamber features a shoulder where the nozzle applies compression to the post-combustion chamber as it threads on to engage all the components and seals in the combustion chamber and prevent movement.

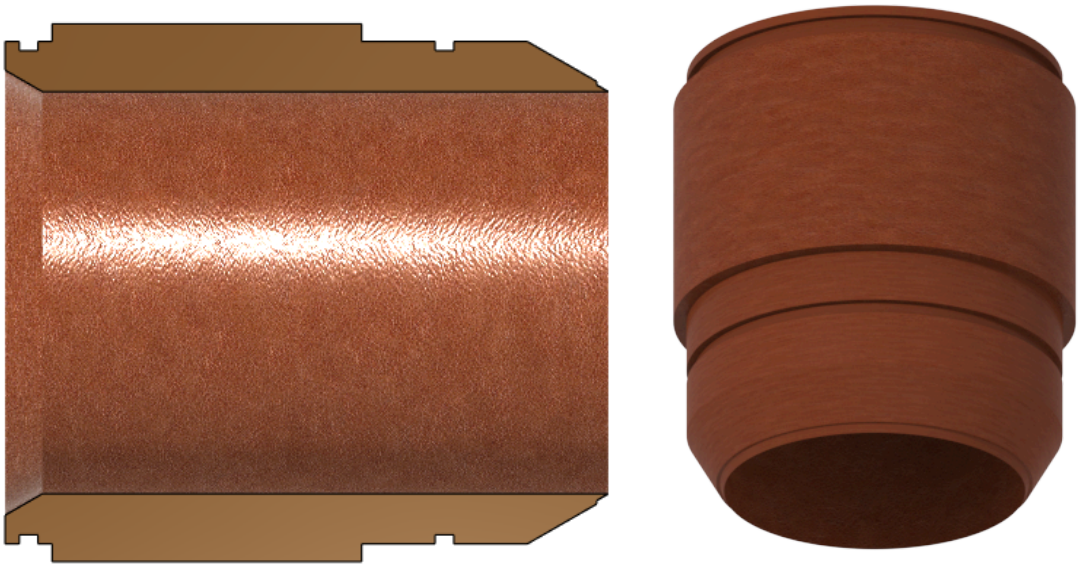

Figure 34: Renders of post combustion chamber

The o-rings on the post-combustion chamber is the same standardised o-ring used on the rest of the combustion chamber and seals in the same way with the nozzle and liner. The 30 degree tapered section of the nozzle outer face will sit in the nozzle converging section to insulate the uncooled section of the nozzle. Furthermore, part of the taper leaves a gap with the nozzle to allow film cooling to exit between the post-combustion chamber and nozzle and fan out to provide immediate and even cooling to the aluminium.

4.10 Resonator

4.10.1 Resonator Overview

Resonators are often used in rocket motors to combat combustion instabilities. There are several main frequencies that are expected to form in the motor; the low frequency hybrid instability, the Helmholtz mode, and the first longitudinal mode. This is evidenced by the peaks labelled in figure 35 below.

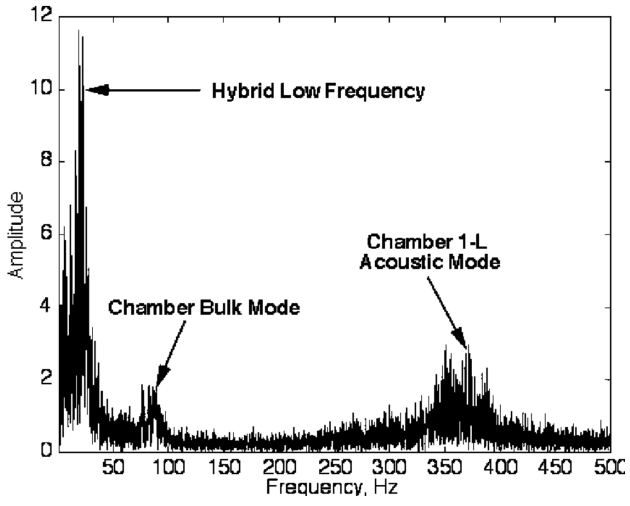

Figure 35: Fourier transform of chamber pressure of NASA Ames Research Center paraffin-based hybrid motor

For Solaris MkIII, the Helmholtz mode frequency was calculated over the changing port diameter and the average frequency from the low frequency band was 79 Hz.

In order to predict the high frequency acoustic mode, research has shown that it can be modelled as a standing wave in a pipe, specifically using the effective length of the post combustion chamber and converging section of the nozzle with closed-open boundary conditions. This led to an expected frequency of 1400 Hz for our engine, and corresponds to the first major peak in figure 36 below.

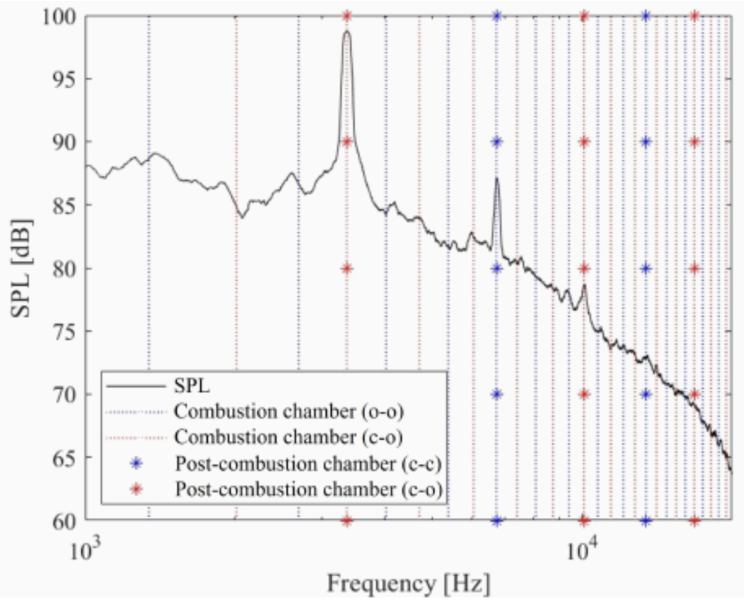

Figure 36: Combustion chamber and post combustion chamber eigenfrequencies plotted over jet noise spectrum

Since Helmholtz resonators are easily sized for higher frequencies due to the size of the resonators increasing with decreasing frequency, they were chosen to be used for the high frequencies caused by the first longitudinal mode. As seen in the figure below, 20 resonators are evenly spaced around the circumference of the chamber just before the fuel grain. The two o-ring grooves are used to seal on the liner and the forward closure.

Figure 37: Resonator assembly

4.10.2 Manufacturing Considerations

In order to machine the cavities of the resonators, two separate parts will be made. The inner section containing the cavities, as seen in figure 38 (left) below, will be machined as a press fit and will sit on the shoulder of the second part. Using conventional sealing methods such as o-rings would not allow for individual sealing of cavities, which is why a press fit was chosen as it allows for partial sealing and a clean interface between the two components which is essential for resonator performance.

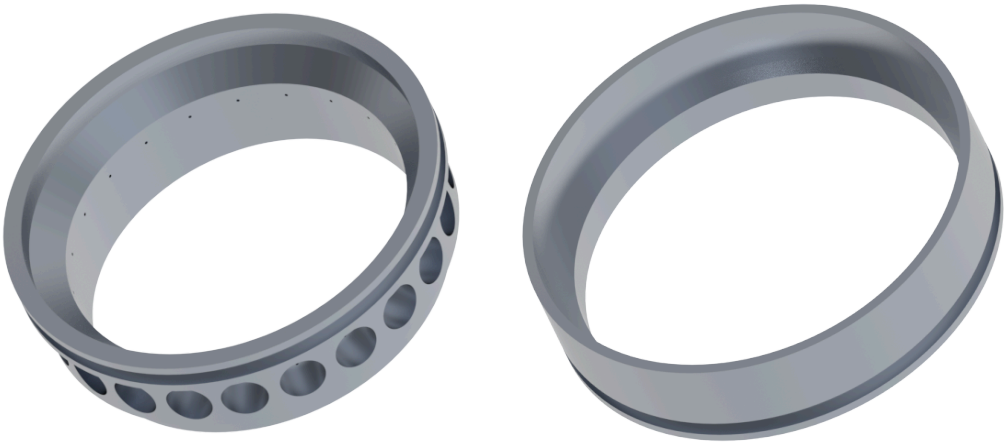

Figure 38: Resonator components, inner ring (left), outer ring (right)

4.11 Fuel insert

4.11.1 Fuel insert overview

A fuel insert will also be used to combat low frequency combustion instabilities, which are typically observed at frequencies under 100 Hz, and are expected to average at 80 Hz with this engine. Fuel inserts are made from a material with a lower regression rate than that of the fuel grain to ensure that the fuel insert burns at a slower rate compared to the surrounding fuel grain. In particular, the fuel insert is planned to have an ABS infill of 30%, higher than the fuel grain's infill of 20%. Due to the higher infill and lower regression rate of the fuel insert, a small step will form as the fuel grain burns away. This step changes the characteristics of the boundary layer, ultimately contributing to more stable and controlled combustion.

One of the important features of the fuel insert design is that it will match the port diameter and design of the fuel grain, ensuring consistency in the flow characteristics of the fuel. To maintain proper orientation, the same cutouts have been used as with the mixing plates. Using this same method means all 3 fuel grains are interchangeable as well as the mixing plate and fuel insert stack up. The matching geometry has been added to both the insert and the fuel grain, as seen in figure 39 below.

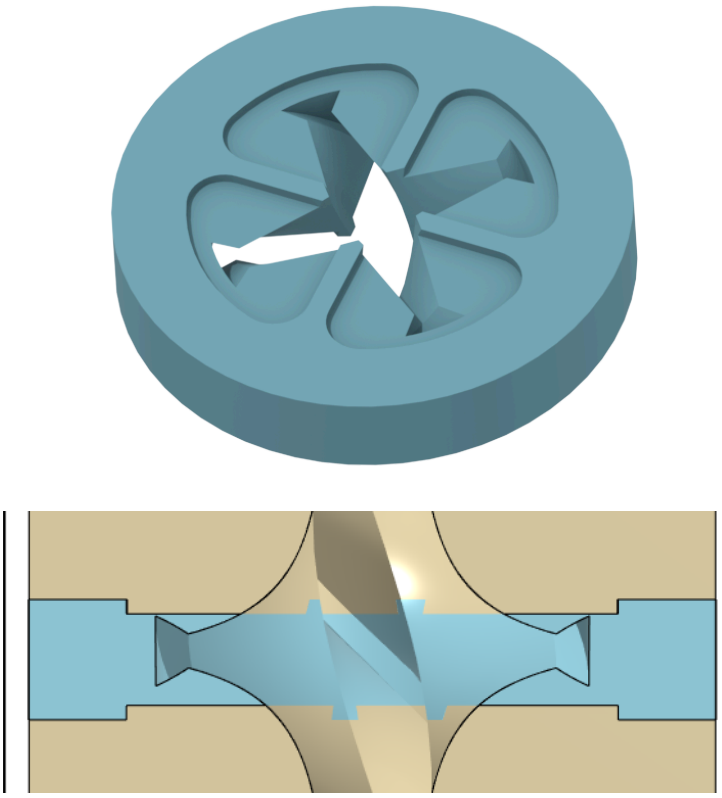

Figure 39: Fuel insert assembly render.

4.12 Ignitor

4.12.1 Ignitor Overview

A torch ignitor was selected as the method of ignition for Solaris MKIII as it was seen as very reliable and repeatable. The team has had trouble in the past igniting with classic in-chamber systems (i.e. solid energetic with e-matches) which prompted us to develop this torch ignitor.

The main design requirements were that the inlet propellant lines be parallel, that it can use different gaseous and liquid propellants (including the H2/O2 supplied at R2S), and that it can sustain ignition at the 10 bar injection pressures of the propellant supply at airborne's facility.

To enable different combinations of propellants (and also injection pressures), the orifice plates have been kept as interchangeable components. This means that each propellant pair will have its own set of orifice plates which are sized using a script, based on RocketCEA, to optimise mass flow rates for desired chamber pressure. See section 6.1.2 for a detailed specification of the ignitor's operating conditions and orifice plate sizes.

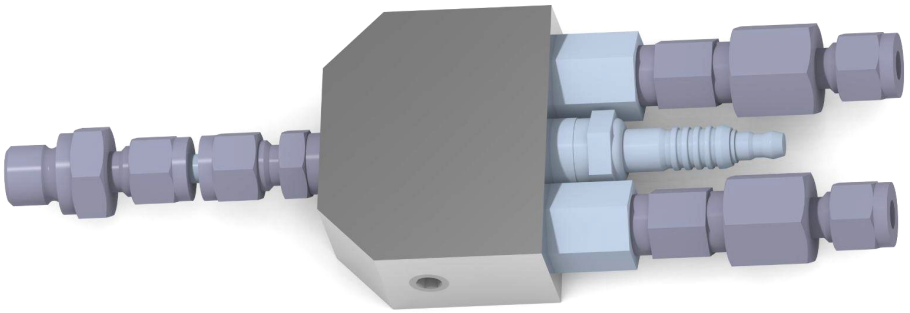

Figure 40: Render of torch ignitor

The ignitor uses an iridium/ceramic spark plug to ignite itself, which is powered through a GSE box designed to output pulses of 15kV at 35mA, built and tested in house by Monash HPR.

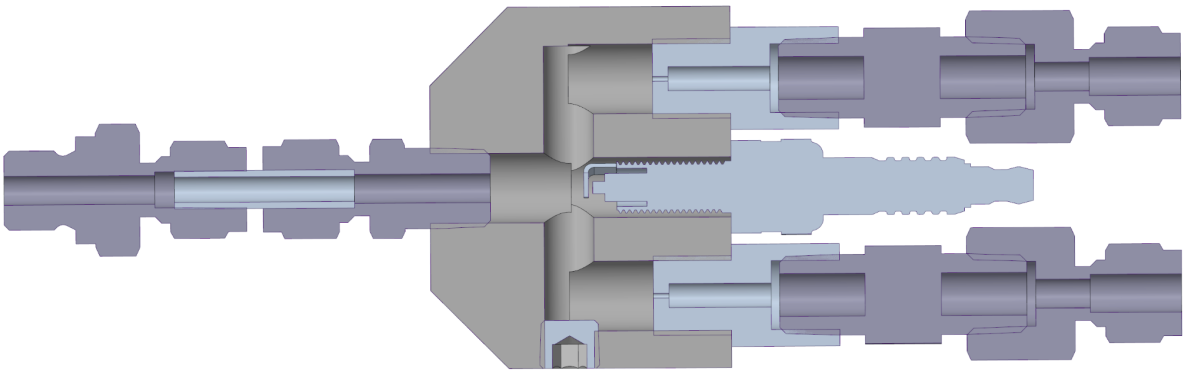

Figure 41: Cross-section of torch ignitor

The ignitor will interface with both injector foreclosures through a G ¼” fitting, as can be seen in the figure below.

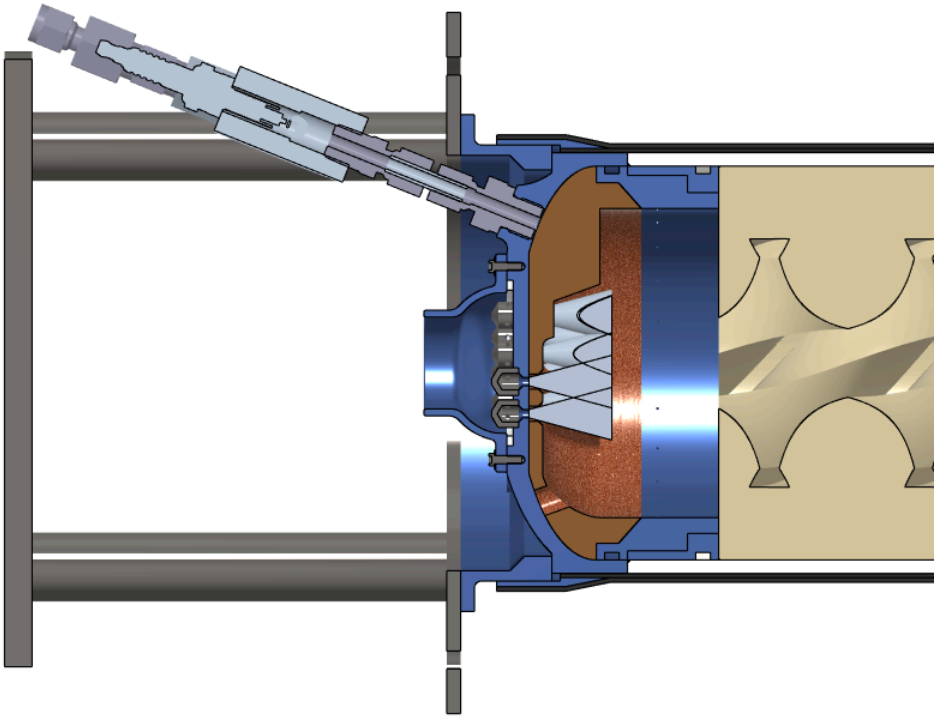

Figure 42: Ignitor cross-section in swirl forward closure

5. Project Timeline

As per figure 43. We are currently in the manufacturing stage of the timeline. We are behind according to this chart, but are ahead of schedule on logistics and the manufacturing stage will occur concurrently with the testing stage. The team is attending IREC 2025 with another hybrid engine and so there will be “stop and start” for each timeline as we switch between projects.

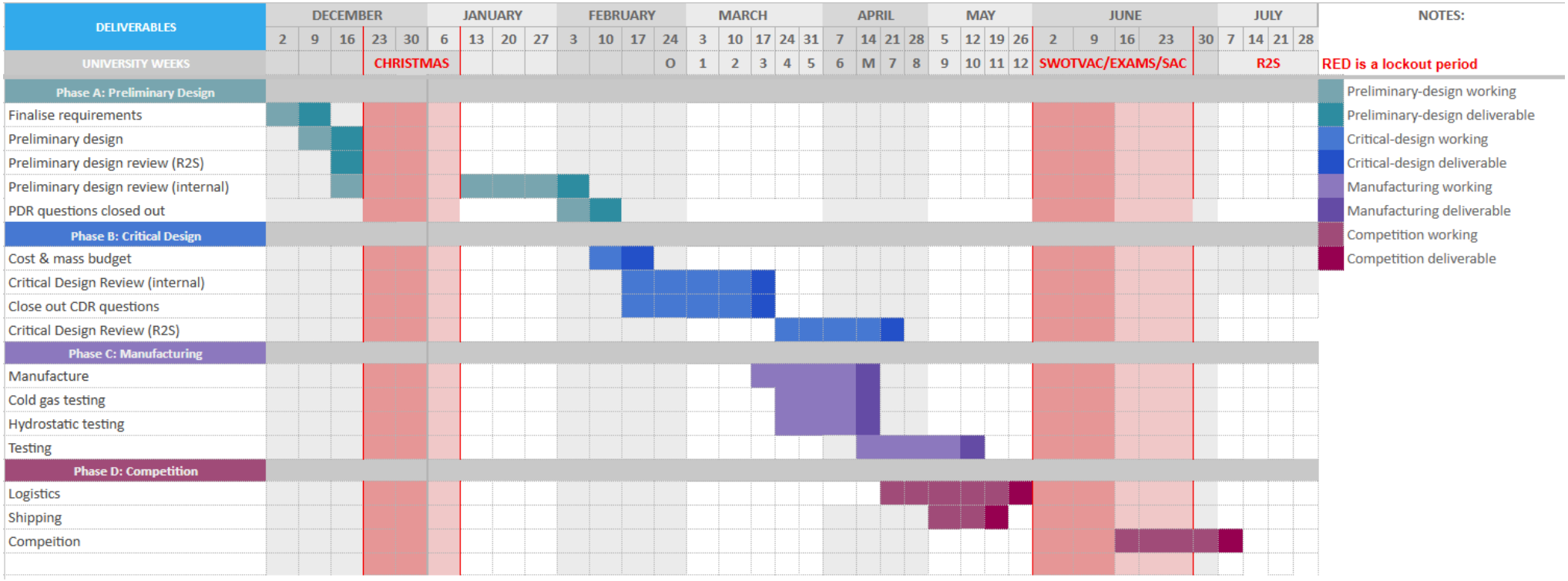

Figure 43: Proposed timeline for Solaris MkIII development between December 2024 and July 2025

6. Design Calculations

6.1.1 Thermodynamic Simulations Engine

Simulations were performed using the team's in-house simulation program. Table 1 represents various inputs and outputs of the simulation. There is some margin in these simulations as they have not been verified for mixing plates or resonators and thus prone to some error, however, can be relied upon as a general approximation and currently are validated against the team's flagship engine Solaris MkII.

The testing plan for the engine will consist of a 4 second combustion hot fire followed by an 8 second combustion hot fire. Both conditions have been modelled.

Parameter/Method/Output	**Value**
Parameters:	
Tank pressure	90 bar
Oxidiser	LOX
Initial port diameter	85mm
Fuel grain outer diameter	140mm
Fuel grain length	700mm (3*270mm)
Fuel grain ABS infill percentage	20%
Fuel grain materials	ABS and Paraffin Wax
Effective tank volume	25L
Nozzle throat diameter	38mm
Nozzle area ratio	10
Effective injector area	86.59 mm^2
Discharge coefficient	0.5
Methods:	
Injector pressure drop and mass flow rate calculation method	*Dyer et al* mass flow rate model. Combination of SPI/SPC and HEM models to form NHEM model.

Combustion calculation method	Rocket CEA python package
Nozzle calculations	Isentropic relations
Outputs (8 second burn):	
Oxidiser mass flow rate	3.56 kg/s
Chamber pressure	58 bar
Chamber temperature	3277 K
Average OF ratio	5.2
Remaining fuel grain (radially)	11.6 mm
Peak thrust	10697 N
Average thrust	8360 N
Impulse	66886 Ns
C*	1500
ISP	200 s
Outputs (4 second burn):	
Oxidiser mass flow rate	3.44 kg/s
Chamber pressure	60 bar
Chamber temperature	3388 K
Average OF ratio	4.3
Remaining fuel grain (radially)	26.3 mm
Peak thrust	10697 N
Average thrust	8741 N
Impulse	34978 Ns
C*	1600
ISP	210 s

Table 1: Simulations parameters, methods and outputs for suggested rocket engine

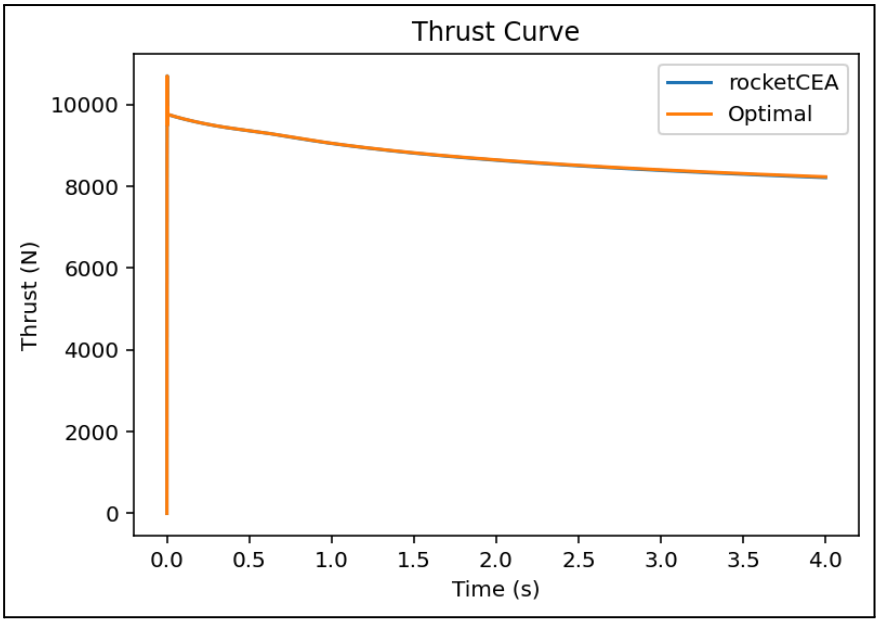

Figure 44: Thrust Curve for 4 second burn

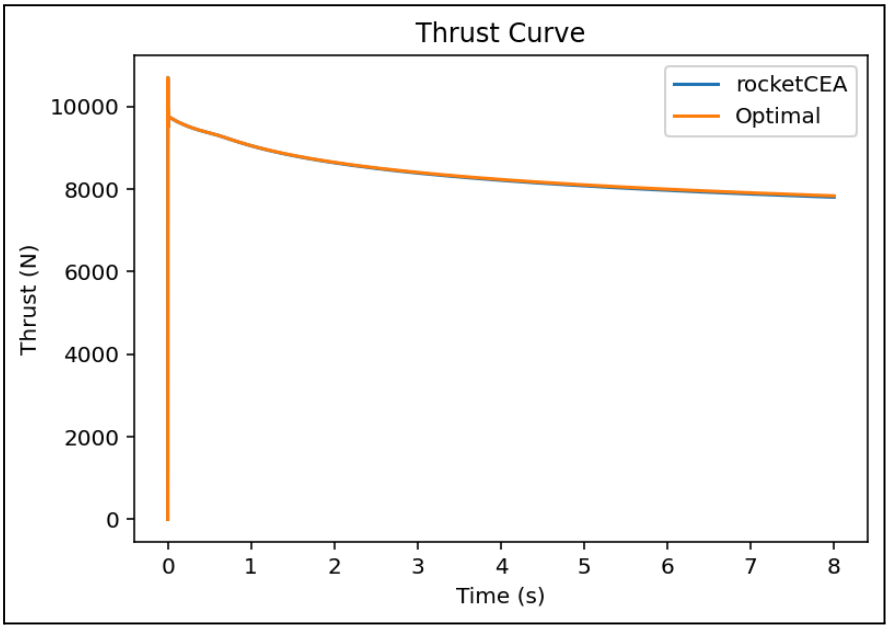

Figure 45: Thrust Curve for 8 second burn

Figure 46: Fuel grain burn contours, simulated in Openmotor

6.1.2 Thermodynamic Simulations Ignitor

Simulations were performed using the team's in-house orifice sizing script based on rocket CEA. Table 2 represents various inputs and outputs of the simulation.

Parameter	**Value**
Oxidiser	Gaseous O2
Oxidiser injection pressure	10 bar
Oxidiser injection orifice diameter	1.20 mm
Oxidiser mass flow rate	3.22 g/s
Fuel	Gaseous H2
Fuel injection pressure	10 bar
Fuel injection orifice diameter	1.60 mm
Fuel mass flow rate	0.80 g/s
Nozzle throat diameter	4.2 mm
Chamber pressure	7 bar
Combustion temperature	2846.28 K
Estimated heat output	96.57 kW

Table 2: Ignitor operating conditions

6.2 Combustion Chamber Simulations and Testing

6.2.1 Chamber Pressure Vessel FEA/ACPs

Combustion chamber structural finite element analysis was run using the Ansys Composite PrepPost and Static Structural applications. Various iterations were conducted as part of this preliminary study to achieve our requirement of a factor of safety greater than 3 on the composite pressure components. Changes made during this process included alterations to the number of plies and their orientation to maximise hoop strength. The final specifications of the composite overwrap are as follows:

Composite Material	Number of plies
Fibreglass 0-90 2x2 Twill Wet	1
3k Carbon Fibre 0-90 2x2 Twill Wet	11
3k Carbon Fibre Sleeve Wet	1

Table 3: COPV plies, weaves and orientations

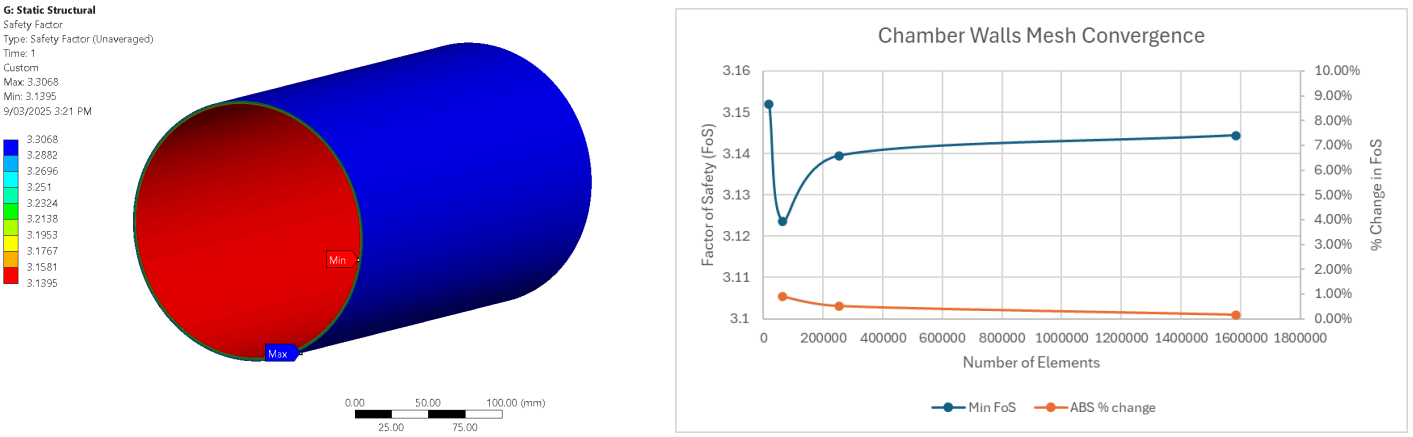

Figure 47: Structural FEA and Mesh Convergence Study results of the combustion chamber COPV

Note that to simplify this analysis, threaded sections of the aluminium couplers were not included in these simulations. Separate calculations for the strength of threaded regions were conducted.

Further exploration of COPV designs will be investigated to achieve greater mass reductions while maintaining a sufficient factor of safety. As shown from figure 46, further optimisation of ply quantities and orientations, be explored further. Our next steps will be to manufacture more test articles to validate simulation results, and then pursue design improvements.

6.2.2 Chamber Pressure Vessel Prototyping

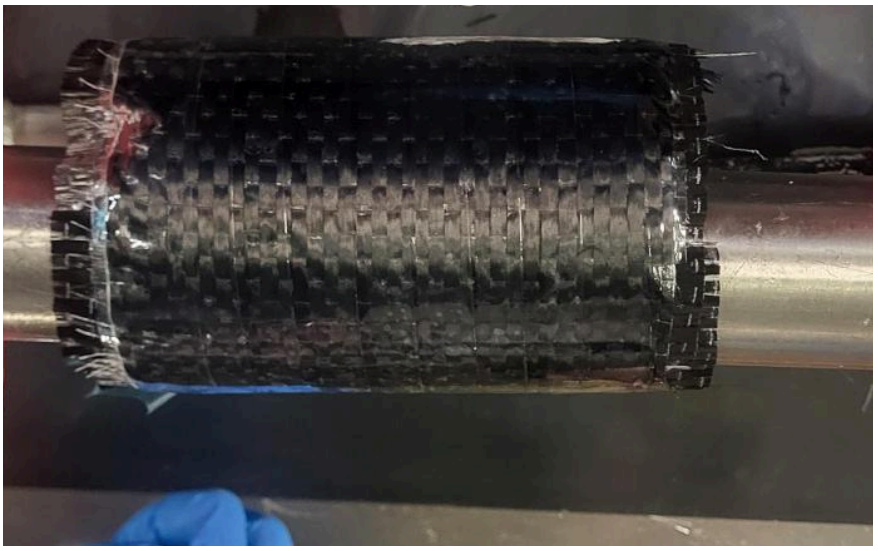

Figure 48: Initial composite overwrapped test article suspended during the wet-layup process

A 60 mm baseline was established to compare manufacturing processes and carbon - Ali bonding preparation. Three 60 mm test articles were produced each using the same baseline setup and dimensions while altering the method of manufacturing, the composite plys, epoxy ratios, couplers and mandrel were kept identical to minimise variation.

60 mm Article 1

The fabrication of Test article 1 began with the layup of a single layer of fiberglass onto the mandel, this was subsequently cured under vacuum pressure of 72 kPa, resulting in a flimsy inner layer. On the following day, aluminum couplers were coated with epoxy and inserted onto the fiberglass tube. A single layer of carbon fiber was then applied with a 20 mm overlap at the bonding interface.

Upon curing, the article exhibited a matte finish (as seen in figure 49), low stiffness and warped easily. This was attributed to excessive epoxy absorption by the breather and peel ply while the article was under vacuum. Which compromised the structure as it was pliable even when handled manually.

During the hydrostatic testing, the initial pressurisation attempt resulted in water permeating through the composite layers. To mitigate this a sealer film was applied to hold the water without leaking. However the second testing failed due to thread shear at the coupler interface, attributed to poorly machined threads.

Figure 49: Final cured 60mm Test Article 1, showing surface conditions and overall geometry

60 mm Article 2

Test article 2 followed the same construction framework as Article 1, the process began with a single layer of fiberglass laid onto the mandrel, followed by the installation of epoxy coated aluminium couplers and the application of a carbon fiber overwrap with a 20 mm step over. The primary modification for this article was the use of heat shrink tape as the consolidation method instead of vacuum bagging.

After the layup was complete, heat shrink was tightly wrapped around the entire length of the article with a 30% step over, followed by a uniform heating to apply even compressive force to consolidate the fibers during curing, this approach minimized the epoxy loss.

Upon curing, the final part exhibited improved stiffness and a smoother gloss finish as seen in figure 50, while fixing the issue of insufficient epoxy some had burned up and became a deformation on the side of the vessel as seen in figure 50. However due to the strong consolidation between the article and mandrel removal without damage was impossible. Consequently hydrostatic testing could not be performed, as the article had to be cut off the mandrel.

Figure 50: damaged composite structure from test article 2

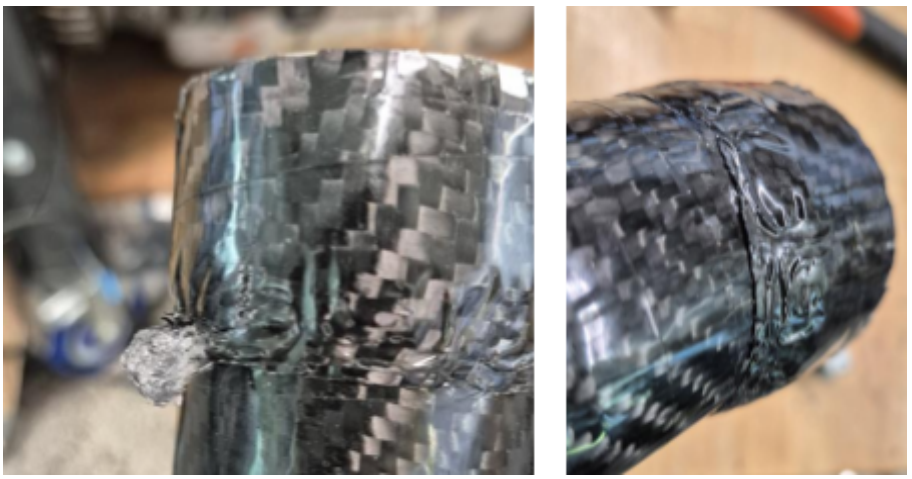

Figure 51: visual inspection of test Article 2,
(left) pooling of epoxy and heat shrink tape.
(right) rippling caused by overheating of heat shrink tape

60 mm Article 3

Test article 3 again used the same setup and layup process as the previous articles, beginning with a single layer of fiberglass laid onto the mandrel, followed by epoxy-coated aluminium couplers and a carbon fiber overwrap with a 20 mm step over. In this iteration, a vacuum bag film was used in an attempt to act as a large continuous piece of heat shrink, aiming to compress the layup uniformly during curing.

The vacuum bag was tightly wrapped around the composite and heated with the expectation that it would contract similarly to heat shrink tape. However, the film did not shrink as intended, and while it held the layup in place, it failed to provide consistent compression across the surface. Heat shrink tape was then overwrapped with a 30% step over to apply additional curing pressure.

Upon curing, the article exhibited strong rigidity and an improved surface finish. However, due to the inconsistent pressure applied by the vacuum bag layer, some areas were pushed in deeper, resulting in surface valleys and indentation, as seen in figure 52). Despite these imperfections, the article was successfully removed from the mandrel without damage.

Hydrostatic testing was performed and showed no leakage or unexpected failure mode. The pressure test resulted in both a fiber and matrix rupture at 39 bar, this result closely aligned with simulation predictions which estimated an expected failure pressure of 38 bar, supporting the structural validity of simulating the composite using ANSYS Composite PrepPost.

Figure 52: depiction of failure size caused by 39 bar of hydrostatic pressure

6.2.3 Chamber Thread Calculations

Thread shear calculations we completed to ensure M158x2.0 ↧16 wont shear during thrust loading axial forces. The following calculations assume the first thread will take 34% of the load, and each progressive thread will take a gradually reducing load.

Using the roy mech female thread shear area formula:

$$A_s = \pi * n * L_e * S_{s\,min} * \left(\frac{1}{2n} + 0.57735 * (D_{s\,min} - E_{n\,max}\right)$$

Where A_n = the shear area of the female thread, n = the number of threads per unit length, L_e = the length of thread engagement, $D_{s\,min}$ = the minimum major diameter female, $E_{n\,max}$ = the maximum pitch diameter of male thread.

Where the shear area would be:

$$A_s = 701.286\,mm^2$$

The shear force is given by the pressure times area, where F_{axial} is the total axial force, p is the pressure, A is area and r is the radius of the chamber :

$$F_{axial} = p * A = p * \pi r^2$$

Where F_s = shear force on the first thread (assuming it takes 34% of the load):

$$F_s = F_{axial} * 0.34$$

$$F_s = 84000$$

To solve the Factor of Safety use:

$$\frac{S_s}{\left(\frac{F}{A}\right)} = 2.73$$

Where S_s = shear strength.

As the factor of safety for the threads is lower than that of the combustion chamber, there is no risk of a catastrophic chamber failure. Instead, in the event of an overpressure scenario, the threads are expected to fail first, acting as a controlled failure point to release pressure and prevent structural rupture of the chamber.

6.2.4 Forward Closure FEA

Structural finite element analysis of both forward closures were run using the Ansys Static Structural application. After multiple design iterations, a 2:1 elliptical profile was selected for the forward closures to withstand the feed and combustion pressures at a factor of safety of 2. Two rounds of structural analysis were performed on each forward closure using pressure conditions expected during start-up and combustion.

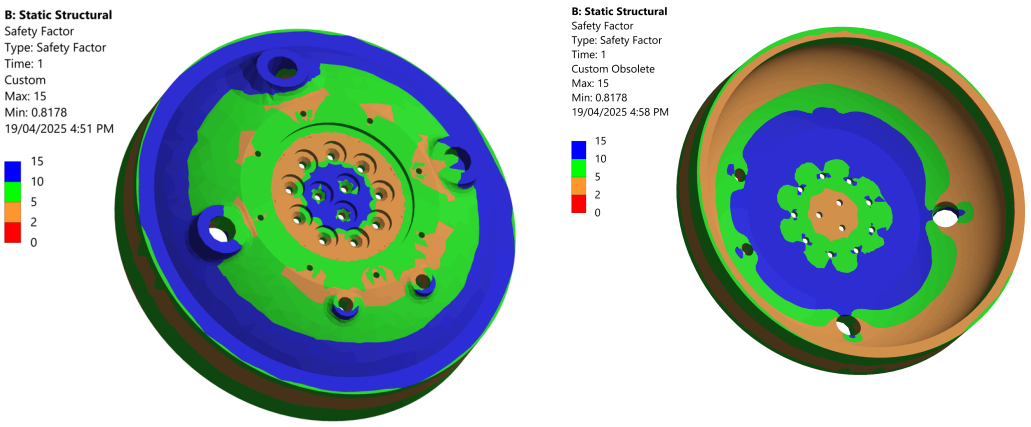

Figure 53: Structural FEA of the swirl injector forward closure

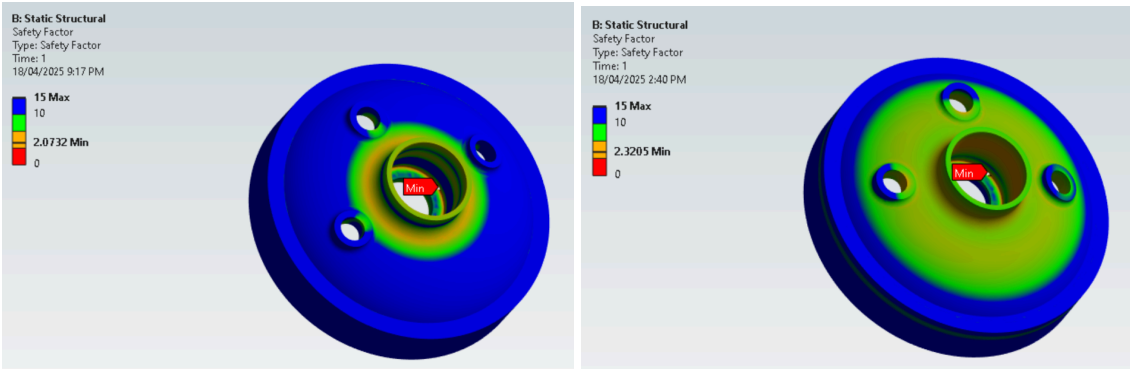

Figure 54: Structural FEA of the pintle injector forward closure during start-up (left) and combustion (right)

6.3 Resonator Calculations

The low frequency instabilities expected were calculated using

$$f = 0.2341(2 + \frac{1}{O/F})\frac{G_0 R T_{av}}{L P_c}$$

Where O/F = oxidiser to fuel ratio, G_0 = oxidiser mass flux, R = gas constant, T_{av} = average temperature, L = fuel grain length and P_c = chamber pressure.

The following plot (figure 55) was produced to model how the low frequency instabilities change throughout the burn. The average of these frequencies was taken and is what will be used as an approximation of the primary oscillation frequency.

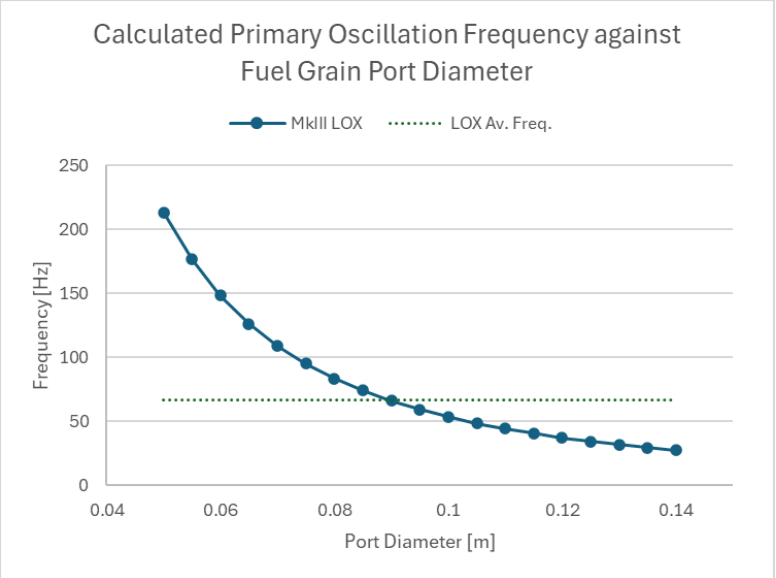

Figure 55: Primary oscillation frequency plotted against fuel grain port diameter

The high frequency acoustic mode was determined using

$$(2n - 1)\frac{c}{4L}$$

Where n = mode index, c = soundspeed and L = post-combustion chamber length.

The Helmholtz resonators were sized with the following equation.

$$f = \frac{c}{2\pi}\sqrt{\frac{A}{VL_{eq}}}$$

Where c = soundspeed, A = port area, V = cavity volume and L_{eq} = equivalent length.

6.4 Engine Mount Calculations

6.4.1 Engine Mount FEA

Figure 56 shows the mounting plate attached to the engine adapter to meet the requirement of a minimum FoS of 2 for non composite components. The loading applied to this was 10 kN and a moment calculated from the masses and distances determined in CAD (Creo parametric 8). The mount is therefore expected to withstand these loads.

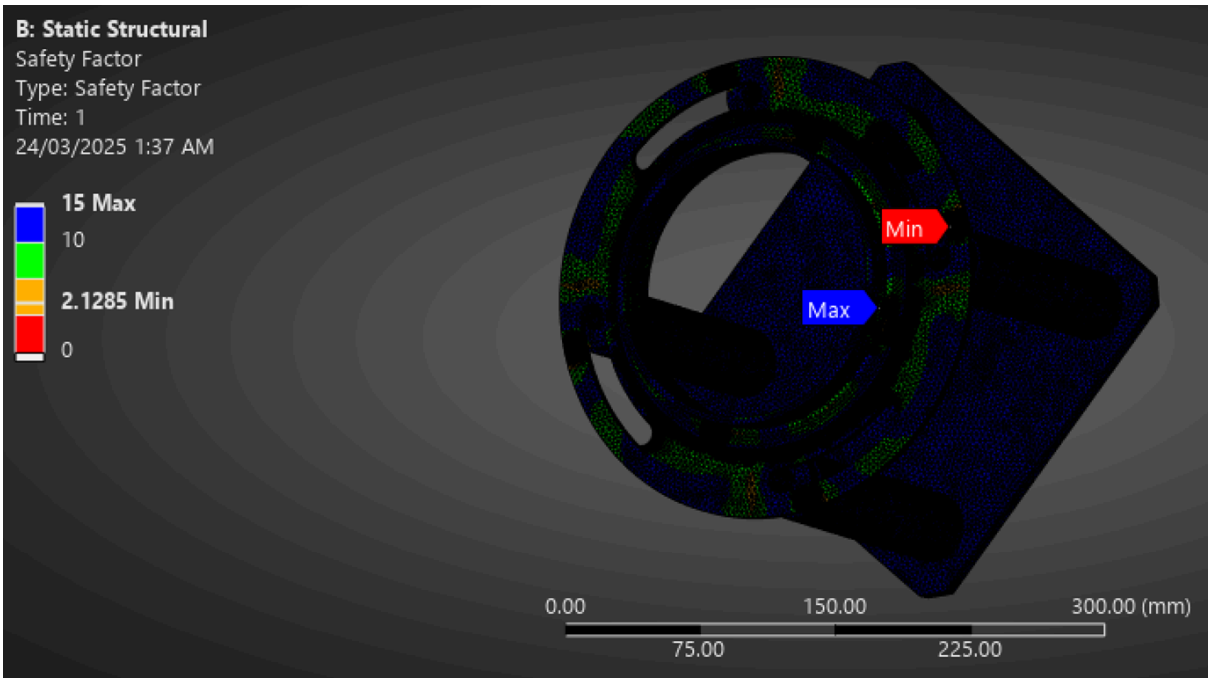

Figure 56: Ansys FEA of engine mount with minimum FoS of 2.13

6.4.2 Bolt Shear Calculations

Bolts shear calculations were also conducted to ensure the chosen 1.5 mm pitch threads with 5 threads of engagement resist the thrust loading, The calculations below determine the threads will not fail. All threads are assumed to be Al 6061-T6 or equivalent alloy (6082 T6).

Effective area given by

$$A_s = \pi/4 * D_s * n * p$$

Where Ds is the major pitch diameter, n is the number of engaged threads, and p is the pitch
Given a major diameter of 150 mm, 5 threads of engagement and pitch of 1.5 mm.

$$A_s = 883.57\ mm^2$$

Considering a max thrust of 10kN, the stress over the threads is:

$$\mu = F/A = 10000/883.57 = 11.317\ MPa$$

Bolt shear calculations were also conducted on the M5x0.8 bolts securing the engine plate to the engine adapter assembly to ensure resistance to moment and thrust loading of the engine.

$$Effective\ Area\text{:}\ A_s = \pi/4\ * D_s = 19.635\ mm^2$$
$$Shear\ stress\text{:}\ \tau = (F/n)/A_s = 2.73\ MPa$$

Where F is moment loading and n is number of bolts using 214.5N loading and 4 bolts.

$$Tensile\ stress\text{:}\ \sigma = (F/n)/A_s = 127.3\ MPa$$

Where F is tensile force and n is the number of bolts using 10 kN thrust loading and 4 bolts.

Further calculations were done to ensure threads remain resistant to shearing under operation.

$$Thread\ Shear\ Area\text{:}\ A_{th} = \pi/4\ * D_s\ * t\ *\ n\ = 78.54\ mm^2$$

Where n is the number of threads and t is the thread engagement depth using 4 bolts and an engagement depth of 5 mm.

$$Shear\ stress\text{:}\ \tau = F/A_{th} = 127.3\ MPa$$

Since the yield stress of Al6061-T6 is 276 MPa, the threads will not fail.

6.5 Mixing Plate Simulations

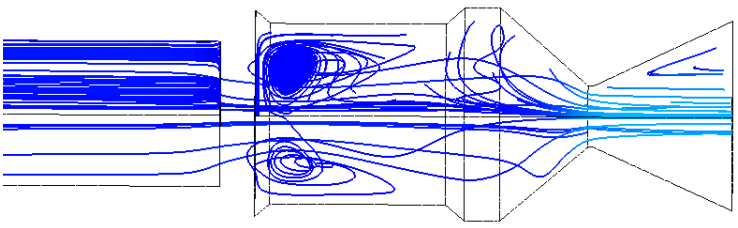

Figure 57: Streamlines after the second mixing plate from multiphase CFD showing a recirculation region

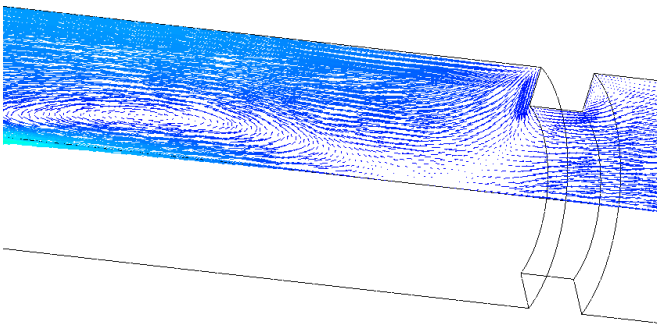

Figure 58: Velocity field before a fuel insert from multiphase CFD

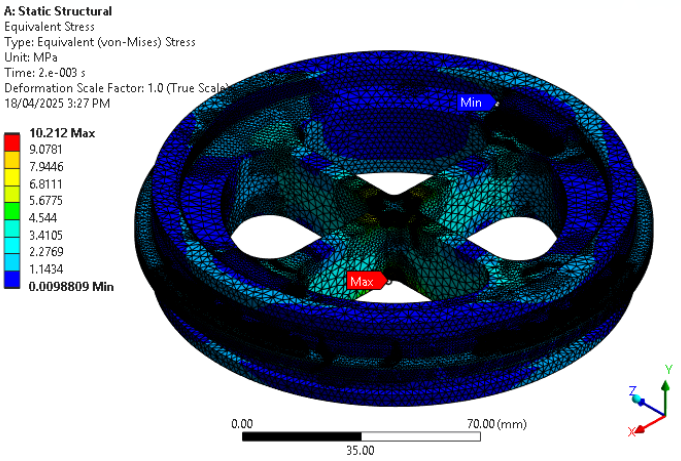

Figure 59: Ansys FEA of the mixing plate with a maximum stress of 10.2 MPa

6.6 Nozzle simulations

6.6.1 Nozzle CFD

Simulating at 8 kg/s of water at 20 bar (2MPa).

Boundary conditions:

nozzle inlet: pressure inlet

- gauge pressure - 60 bar (6 MPa)
- supersonic pressure - 59.9 bar (5.99 MPa), this equates to an inlet velocity of 17m/s that was given to fluent as an initial value, but fluent solved it to be around 78 m/s
- total temp - 3100 K

nozzle outlet: pressure outlet

- gauge pressure - 0 (ground level atm)

- total temp - 1200 K (not used unless backflow occurs)

cooling inlet: mass flow inlet

- 8 kg/s
- 20 deg celsius
- supersonic pressure not used unless cooling inlet is supersonic

cooling outlet: pressure outlet

- 20 bar (2 MPa)
- 80 deg celcius (353 K) - not used unless backflow

Initialisation: FMG with 5 grid levels

Calculations: 604 iterations

Convergence Criteria: 5 point temp probes, 4 area/volume-weighted temp monitors

Results:

Surface monitors converged values:

- throat wall temp: 424.3 K (151.15 Celsius)
- near outlet wall temp: 333.6 K (60.45 Celsius)
- near inlet wall temp: 624.3 K (351.15 Celcius)
- between throat and outlet temp: 344.2 K (71.05 Celsius)
- between throat and inlet temp: 352.7 K (79.55 Celsius)

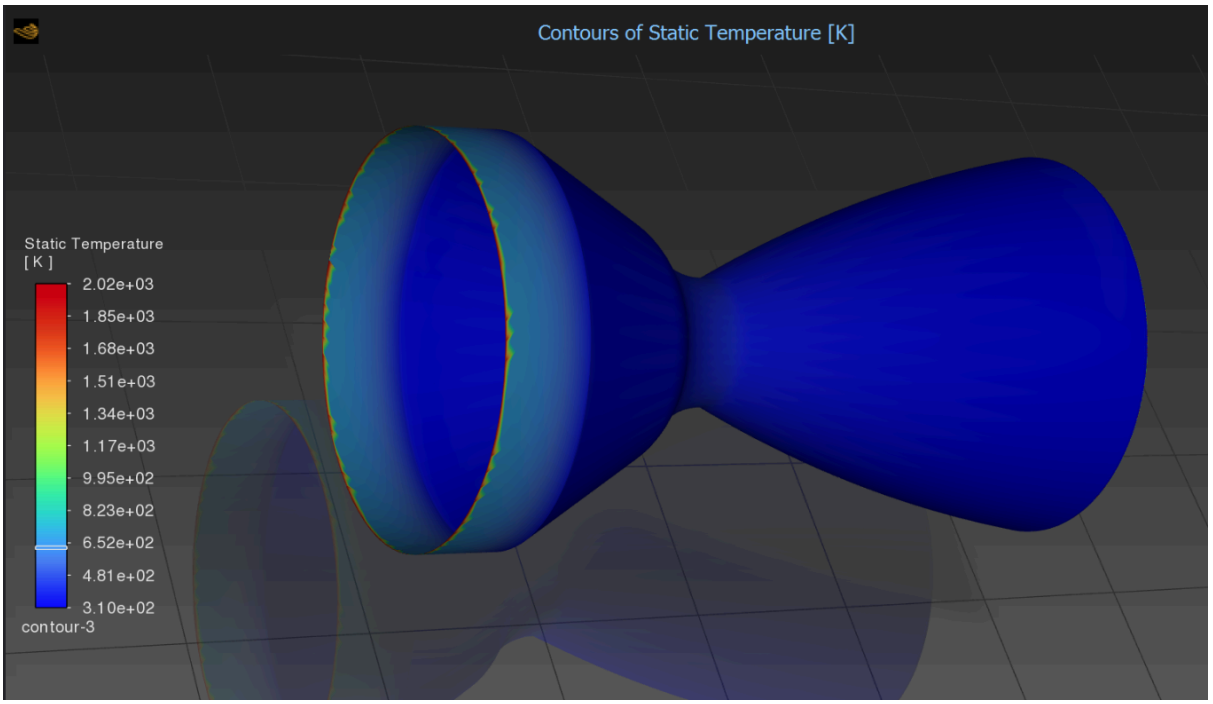

Figure 60: Contour plot of nozzle inner wall surface temperatures

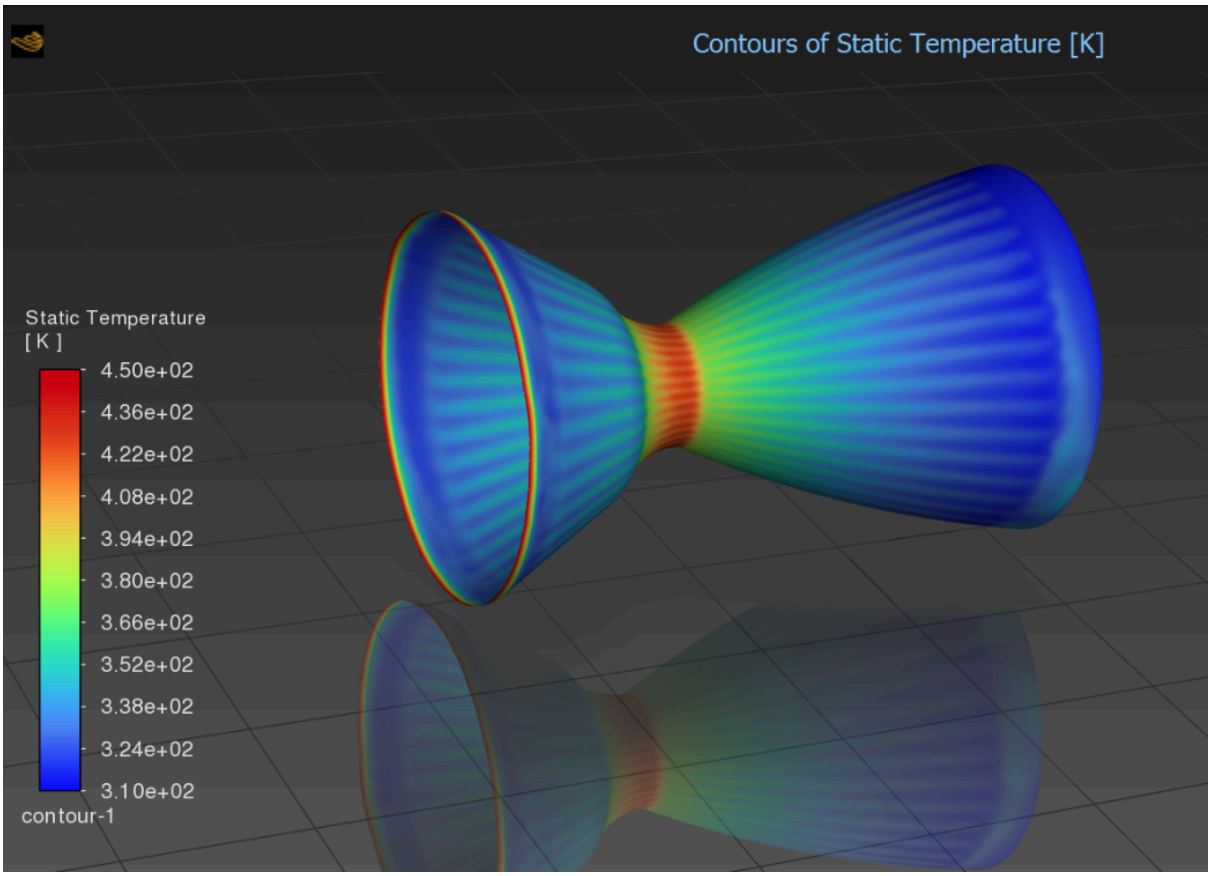

Figure 61: Contour plot of nozzle channel surface temperature

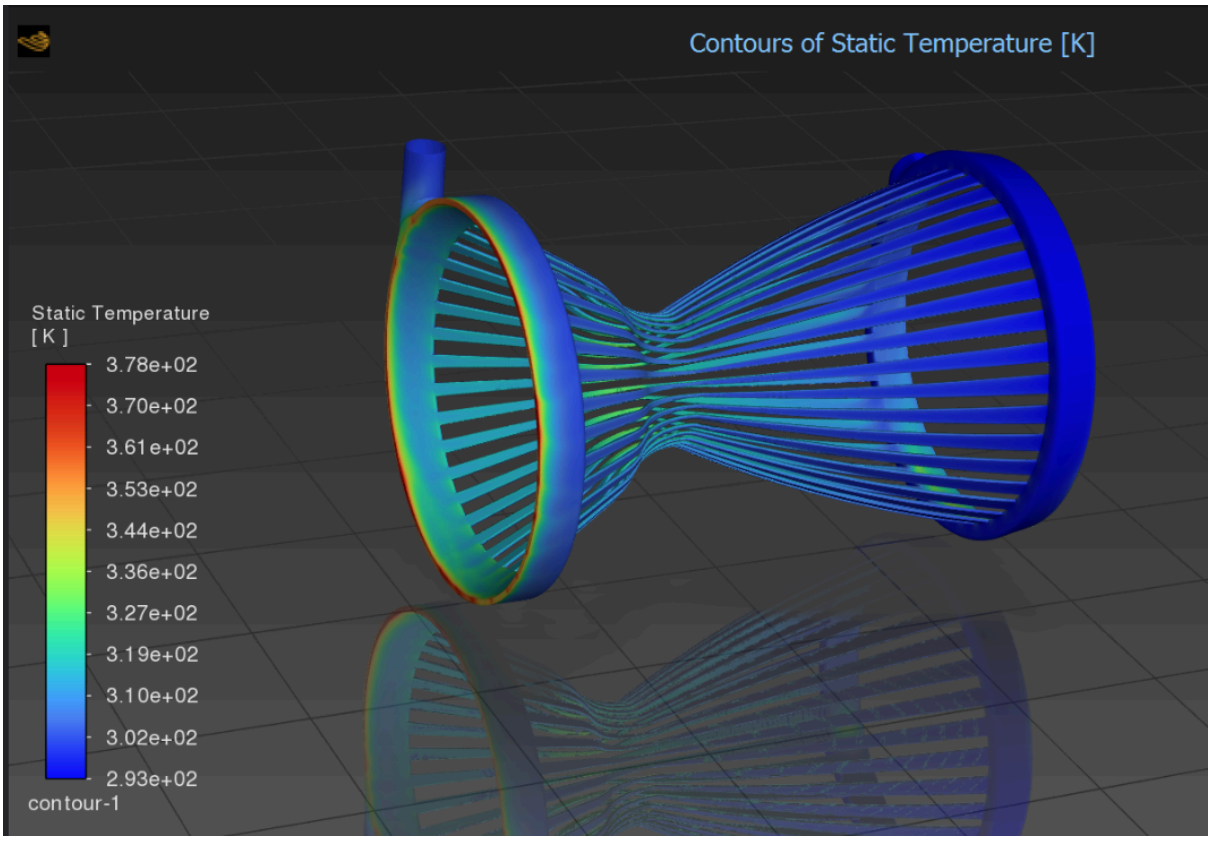

Figure 62: Contour plot of nozzle channel temperatures

6.6.2 RPA and MATLAB Calculations

The following calculations were performed in RPA and MATLAB (using Bristol SEDS script):

	Water low pressure	Water high pressure
Thermal conductivity W/(m K)	165	165
Inner wall thickness (mm)	2.5	1.5
Rib height (mm)	2	1
Channel width 1 (mm)	7	7
Channel width min (mm)	1.7	1.7
Channel width 2 (mm)	4.4	4.4
Number of channels	40	40
Helix angle (deg)	25	25

Coolant temperature (K)	300	300
Coolant pressure (bar)	20	75
Coolant mass flow rate (kg/s)	8	1.3
Film cooling location 1 (mm)	50	60
Film cooling location 2 (mm)	-	120
Mass flow rate 1 (kg/s)	3.1	0.45 kg/s
Mass flow rate 2 (kg/s)	-	0.27 kg/s

Table 5: Water cooling parameters for RPA

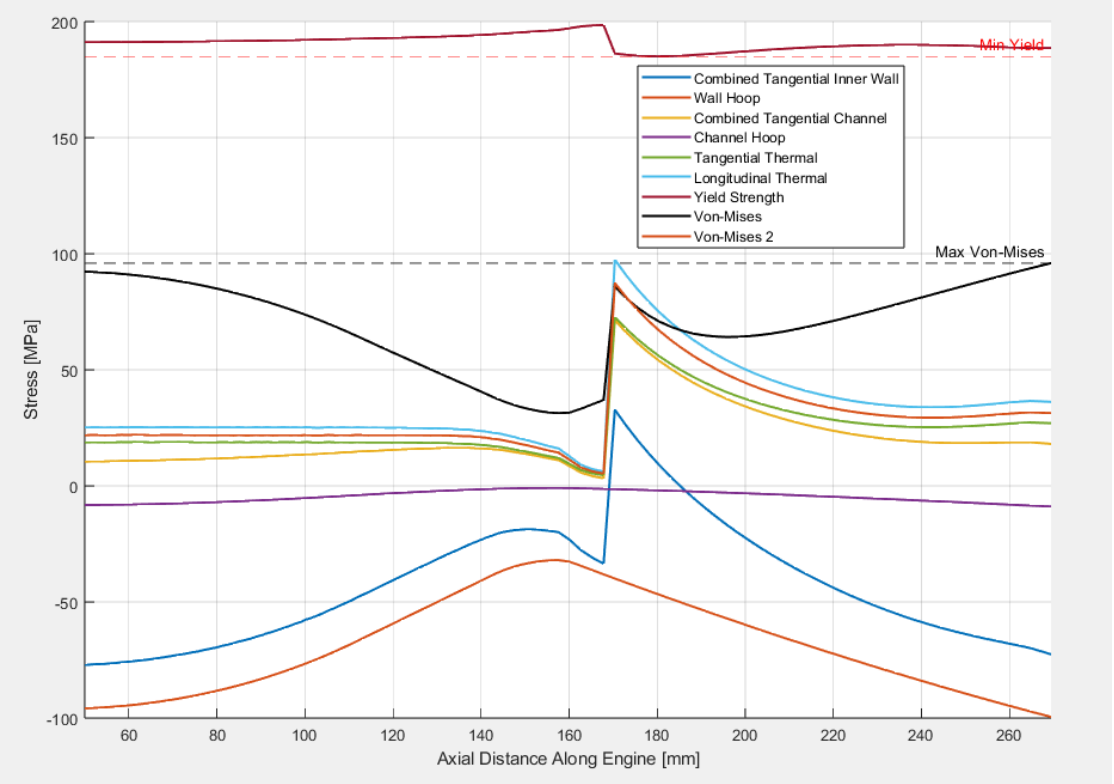

Figure 63: Stress as a function of axial distance down the nozzle (low pressure water)

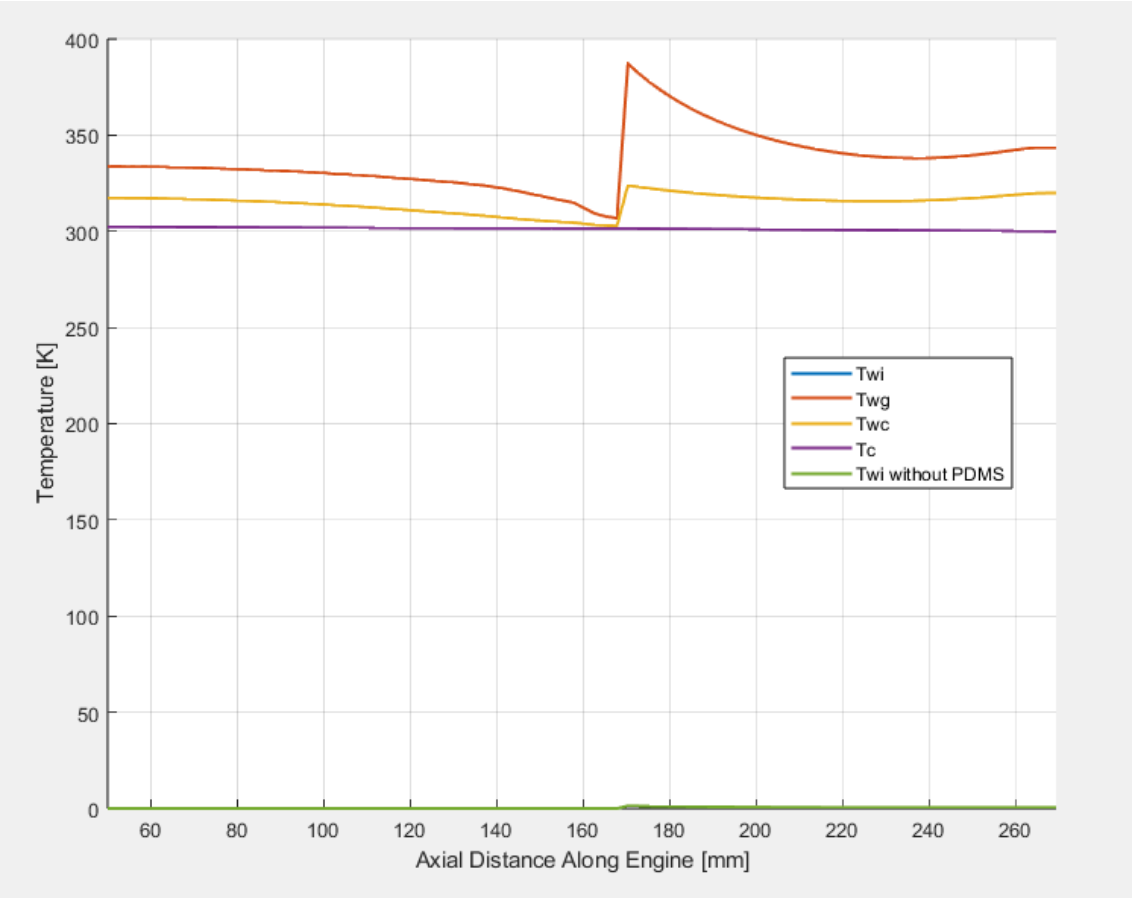

Figure 64: Nozzle temperature on different surfaces vs axial distance down the nozzle (low pressure water)

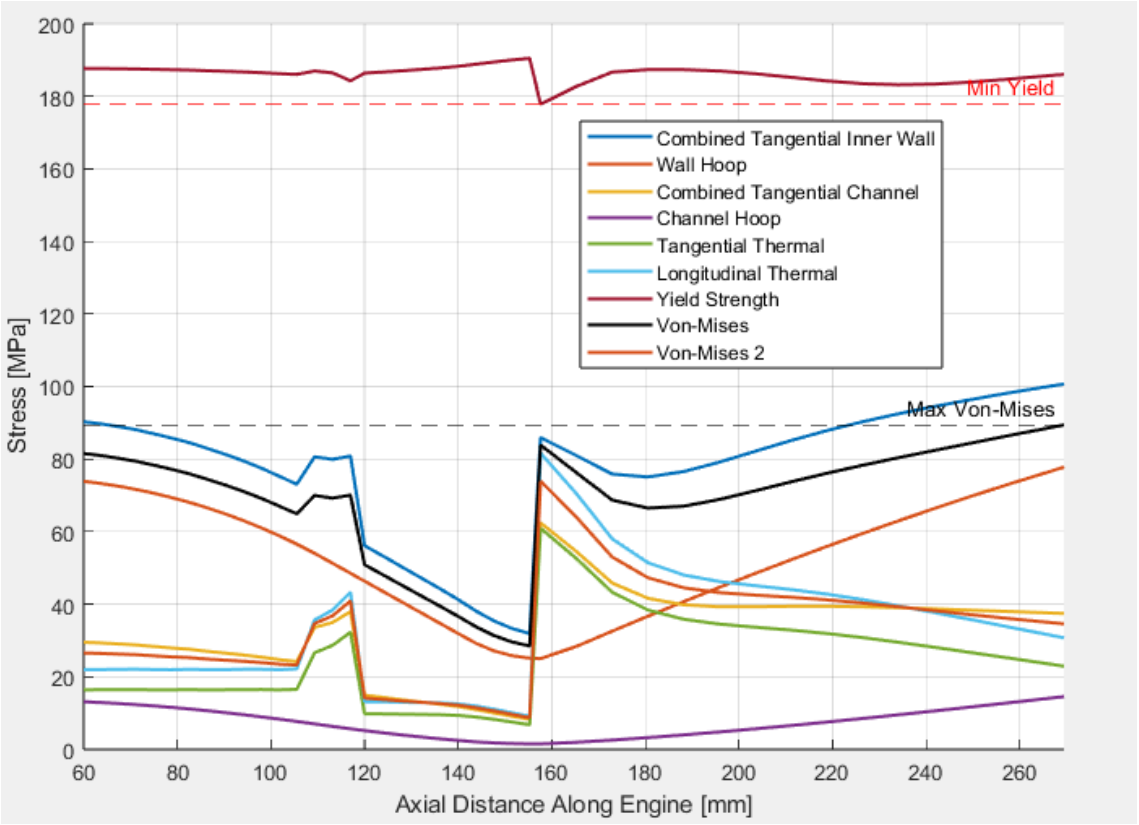

Figure 65: Stress as a function of axial distance down the nozzle (high pressure water)

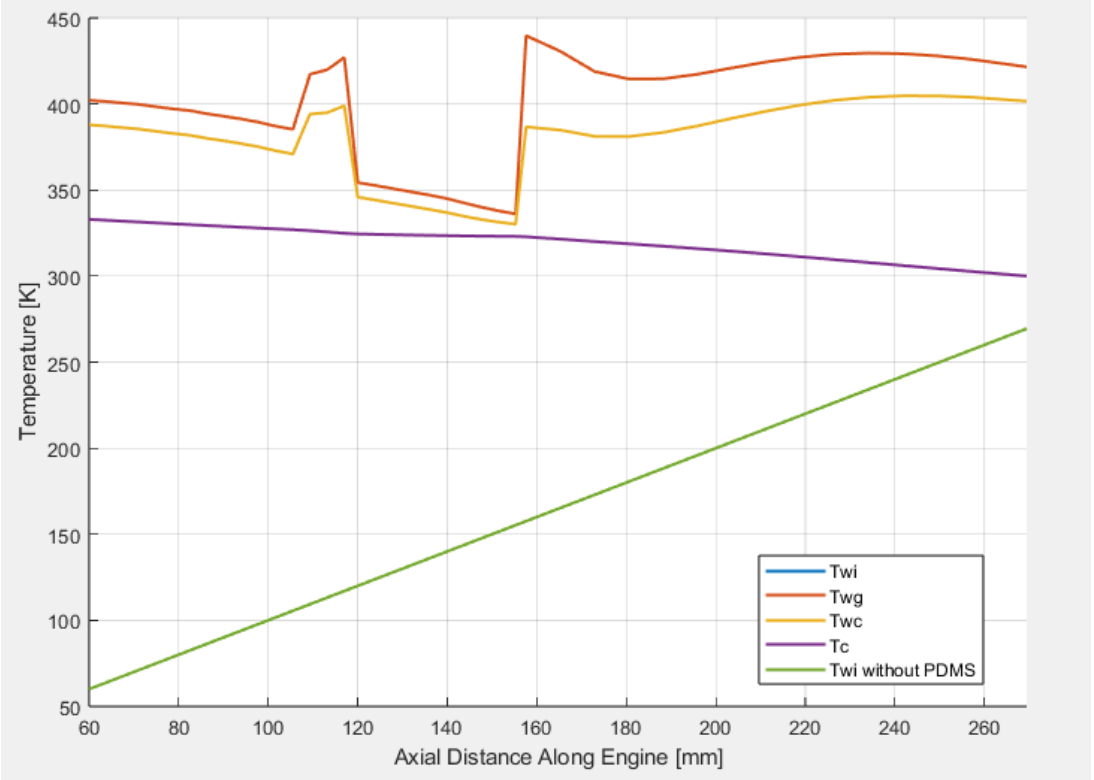

Figure 66: Nozzle temperature on different surfaces vs axial distance down the nozzle (high pressure water)

7. Safety

Safety is of the utmost importance for any engineering undertaking and this project is no exception.

Due to the nature of composite vessels and the difficulty of accurate simulation, a safety factor of 3 is used for all composite components. All other components will require a safety factor of 2.

Each component will be hydrostatically tested to 1.5 MEOP (Maximum Expected Operating Pressure) to ensure they are safe to use during a test fire. Hydrostatic testing will also be used to ensure sealing of important components. Risk assessments and Safe Work Instructions will be developed for the system to ensure the proper information is available for anyone handling the engine.

Hazard Analysis is conducted according to the standards dictated by WorkSafe Victoria and enforced by Monash University. In accordance with these standards, individual hazards and their associated risks are quantitatively assessed under the following Matrix

	Severity of Consequences				
Likelihood of Event	Insignificant	Minor	Moderate	Major	Catastrophic
Almost Certain	Significant Risk	Significant Risk	Significant Risk	Extreme Risk	Extreme Risk
Likely	Moderate Risk	Significant Risk	Significant Risk	Significant Risk	Extreme Risk
Moderate	Low Risk	Moderate Risk	Moderate Risk	Significant Risk	Significant Risk
Unlikely	Low Risk	Low Risk	Moderate Risk	Moderate Risk	Significant Risk
Rare	Negligible Risk	Low Risk	Low Risk	Moderate Risk	Moderate Risk

Table 6: Risk Matrix for analysis of risk likelihood and severity

In the context of this table, an insignificant hazard would result in an injury requiring no treatment, a minor hazard would require first aid treatment for minor injuries, a moderate hazard would require professional medical treatment, a major hazard would require hospital admission, and a catastrophic hazard would result in a fatality or permanent disabling injury.

Hazard	Possible Causes	Risk of Mishap/ Consequence	Mitigation Approach	Risk of injury after mitigation
Storage and handling of E-matches.	Static discharge prematurely igniting e-match.	Low Risk: Unplanned ignition of e-match may ignite nearby e-matches, flammable material or other energetic devices.	E-matches are always stored with twisted ends, shorting the path through the e-match so static cannot accumulate on terminals. E-matches are stored separately from any flammable or explosive material.	Negligible
Explosion of Combustion Chamber	Blockage of nozzle. Overpressurisation of combustion chamber. Cavitation in fuel grain. Excessive heat weakening chamber wall.	Moderate Risk: Whilst the likelihood of combustion chamber explosion is low, the consequence is substantial, with shockwaves and shrapnel posing a substantial danger to personnel.	The combustion chamber will be inspected for foreign objects prior to assembly. The nozzle threads are designed with a lower factor of safety than chamber walls to ensure the engine fails in a safe manner. The combustion chamber shall be thoroughly tested to ensure that there is no risk of overpressurisation. An insulating liner shall be inserted between the fuel grain and liner.	Moderate
Ignition of fuel grain during transportation.	Heat and an ignition source during transport may cause the fuel grain to begin burning	Low Risk: Paraffin wax requires substantial and continuous heat to burn and burns relatively energetically compared to a solid motor.	Fuel grains will be transported in an appropriate wooden container, shielded from heat and segregated from sources of ignition.	Negligible
Burnthrough of nozzle	Blockage of regenerative cooling channels. Insufficient regenerative cooling flow rate. Insufficient conduction through nozzle	Moderate risk: Whilst the likelihood of nozzle burnthrough is low, the consequences are substantial, as this will cause LOX to flow into the engine exhaust.	After printing, the nozzle shall be shaken rigorously on a shaker table to loosen and remove any particles in the cooling channels. The nozzle will be heated and cold air put through the channels and thermal imaging will reveal any blockages. Furthermore, x-ray or CT imaging will be investigated.	Moderate

	wall.		The nozzle fluid flow and heat transfer shall be thoroughly modelled with a generous factor of safety to ensure there is sufficient cooling.	
Premature ignition of oxidizer	Combustible particulates in the LOX flow path External heat sources warming the LOX flow path	Moderate Risk: Whilst the likelihood of premature oxidizer ignition is low, the consequence is substantial, with shockwaves and shrapnel posing a substantial danger to personnel.	Clean all engine components with high pH detergent and store in PTFE lined bags inside a moisture barrier bag prior to testing.	Moderate
Structural Failure of Injector	Manufacturing defects cause failure. Thermal shock cracks the injectors.	Moderate Risk: Likelihood is low, the consequence would be a loss of thrust or in a rare case loss of engine.	The injector assembly will be hydrostatically tested prior to static fire and all parts will be measured by the machinist and another person to ensure correct dimensions.	Low

8. Test Fire Procedures

Assembly and testing checklists will be developed and refined so that any team member could complete assembly & hot-fire preparation by following these clear instructions.

Engine assembly and operation checklists, will be attached to this submission and sent to the relevant parties.

The engine is designed to be assembled prior to the testing day. The fuel grains will be cast and the segments will be assembled with fresh o-rings and grease. Cleaning procedures will also be developed to ensure no unwanted corrosion occurs from the oxidiser.

The engine will be assembled, checklists will be performed and it will then be mounted to the AEL J1 test facility via the low thrust setup with the high thrust load cell. We will use a 1 inch BSP parallel thread to connect to the test facilities fluid lines. The engine will be mounted to the M12 6 inch square plate using the standoffs to allow for ignitor, sensor and fluid access. The team has its own ignitor system but will design the engine such that it can use the organisers' torch ignition system.

Time permitting the team would look at conducting a half length test fire first, followed by two full length test fires to gain valuable data on the engine. Ideally the team would test with their own new ignition system currently in development and would do so depending on time and availability. (see table 7)

Test Description	Configuration	Burn duration
Solaris MkIII Hot fire	Supply oxidiser: - LOX - 90 bar - 3.44 kg/s Nozzle: - Water - 1.3 kg/s - 75 bar Swirl injectors	4s
Solaris MkIII Hot fire	Supply oxidiser: - LOX - 90 bar - 3.56 kg/s Nozzle: - Water - 1.3 kg/s - 75 bar Swirl injectors	8s
Test #3		
Solaris MkIII Hot fire (option 1 - time permitting)	Supply oxidiser: - LOX - 90 bar - 3.56 kg/s Nozzle: - Water - 1.3 kg/s - 75 bar Pintle injector	8s
Torch ignitor test (option 2 - alternative)	Supply oxidiser: - O2 - 3.22 g/s - 10 bar Supply fuel: - H2 - 0.8 g/s - 10 bar	3s

Table 7: Monash HPR testing plan

8.1 Test 1 - 4s second burn

This test is considered a half length burn, its function is to be a safe way to characterise the engine. This will be fired in the swirl injector configuration. This shorter burn will ensure we can monitor regression rate for higher than expected regression as well as monitor thermal stresses on the nozzle and chamber and ensure we don't get higher heat transfer than expected.

Critical monitors:

- The regression rate of the fuel grain must be monitored, to ensure it doesn't regress too far beyond expectations and damage the engine.
- Thermal stresses on the nozzle will need to be monitored along with the general temperature to ensure the nozzle can handle its expected steady state loads and will cool as designed.
- The COPV must remain at a reasonable temperature, if too much heat transfer occurs the COPV will fail.
- The resonators, mixing plates, pre-chamber, baffles, fuel inserts and post-chamber must be monitored for ablation to ensure they won't break apart and inject debris in to the exhaust

Insights:

- If the regression rate is above a threshold such that the engine is at risk of burning through the liner for an 8s burn, the burn time will need to be adjusted.
- If the nozzle is showing signs of fatigue, it might have to be cycled out for a different nozzle and burn times adjusted.
- If the nozzle is exceeding temperature expectations beyond a dangerous amount, the nozzle flow rates might need to be adjusted or the burn time capped at 4s.
- If the COPV is approaching its temperature limit, the burn time will need to be re-assessed.
- Gain data on chamber pressure and compare to expectations, potentially adjusting flow rate as needed.
- Observe axial regression and the efficacy of the mixing plates

8.2 Test 2 - 8s second burn

This would be a near full scale burn of the engine. A full scale burn would be 10s. This would be the strongest indication of the overall engine performance and would be what we use to characterise the engine going forward.

Critical monitors:

- The regression rate of the fuel grain must be monitored, to ensure it doesn't regress too far beyond expectations and damage the engine.
- Thermal stresses on the nozzle will need to be monitored along with the general temperature to ensure the nozzle can handle its expected steady state loads and will cool as designed.
- The COPV must remain at a reasonable temperature, if too much heat transfer occurs the COPV will fail.

- The resonators, mixing plates, pre-chamber, baffles, fuel inserts and post-chamber must be monitored for ablation to ensure they won't break apart and inject debris in to the exhaust

Insights:

- Will be able to confirm if the regression rate model which should have been adjusted as a result of test 1 is accurate.
- The nozzle data at close to steady state temperatures will be invaluable for our next designs.
- If the nozzle is exceeding temperature expectations beyond a dangerous amount, the nozzle flow rates might need to be adjusted or the burn time decreased.
- If the COPV is approaching its temperature limit, the burn time will need to be re-assessed.
- Gain further data on chamber pressure as a function of the shifting O/F ratio and compare to expectations, potentially adjusting flow rate as needed.
- Observe axial regression and the efficacy of the mixing plates

8.3 Test 3 - 8s second burn - pintle injector

This will be the same parameters as test 2, but with the pintle injector. This hopes to characterise the performance of swirl vs pintle injectors in a cryogenic hybrid to develop a benchmark.

Critical monitors:

- Regression around the injector and the effect of injector choice on axial regression.
- Chamber pressure and instabilities compared to the swirl injector.
- Same safety monitors as test 2.

Insights:

- Provide direction on which injector category to pursue further, based on efficiency, combustion instabilities and axial regression.
- Gain further data on the engine and the consistency of its performance.
- More data on O/F shift and burn characteristics.

8.3 Test 3 - Alternate - Torch ignitor test

This will be a test of the teams own torch ignitor. Will be an ignition test and might involve tweaking of orifice plates, supply parameters and ignition timing to get the most consistent flame.

Critical monitors:

- Damage to the ignitor from heat.
- Stability of the flame
- Temperature and length of the torch flame

Insights:

- Provide data for the team to use and tune the ignitor with.
- Give the necessary thermodynamic performance to best use it to ignite an engine in the future.
- Give insight into the longevity of the body on repeat tests.